BMP-regulated exosomes from *Drosophila* male reproductive glands reprogram female behavior

Laura Corrigan,[1] Siamak Redhai,[1] Aaron Leiblich,[1,2] Shih-Jung Fan,[1] Sumeth M.W. Perera,[1] Rachel Patel,[1] Carina Gandy,[1] S. Mark Wainwright,[1] John F. Morris,[1] Freddie Hamdy,[2] Deborah C.I. Goberdhan,[1] and Clive Wilson[1]

[1]Department of Physiology, Anatomy and Genetics and [2]Nuffield Department of Surgical Sciences, University of Oxford, Oxford OX1 3QX, England, UK

Male reproductive glands secrete signals into seminal fluid to facilitate reproductive success. In *Drosophila melanogaster*, these signals are generated by a variety of seminal peptides, many produced by the accessory glands (AGs). One epithelial cell type in the adult male AGs, the secondary cell (SC), grows selectively in response to bone morphogenetic protein (BMP) signaling. This signaling is involved in blocking the rapid remating of mated females, which contributes to the reproductive advantage of the first male to mate. In this paper, we show that SCs secrete exosomes, membrane-bound vesicles generated inside late endosomal multivesicular bodies (MVBs). After mating, exosomes fuse with sperm (as also seen in vitro for human prostate-derived exosomes and sperm) and interact with female reproductive tract epithelia. Exosome release was required to inhibit female remating behavior, suggesting that exosomes are downstream effectors of BMP signaling. Indeed, when BMP signaling was reduced in SCs, vesicles were still formed in MVBs but not secreted as exosomes. These results demonstrate a new function for the MVB–exosome pathway in the reproductive tract that appears to be conserved across evolution.

Introduction

In addition to sperm, seminal fluid contains multiple factors secreted by male reproductive glands that activate sperm (Rodríguez-Martínez et al., 2011) and can influence female physiology and behavior (Kershaw-Young et al., 2012). In *Drosophila melanogaster*, the paired accessory glands (AGs) secrete peptides that perform such functions (Wolfner, 1997). Sex peptide (SP) is one key product that in females can induce enhanced egg laying (Chapman et al., 2003), gradual release of sperm from storage organs (Liu and Kubli, 2003; Peng et al., 2005; Avila et al., 2010), and reduced receptivity to remating (Chen et al., 1988). This latter effect directly conflicts with female reproductive interests, leading us to investigate whether males use unconventional signaling strategies to achieve this.

Each AG is composed of a monolayered epithelium encased by a muscular sheath, which contracts during mating to expel the luminal contents. The epithelium is composed of two distinct binucleate cell types (DiBenedetto et al., 1990; Bertram et al., 1992). There are ∼1,000 main cells (MCs), which secrete signaling proteins such as SP (Chapman et al., 2003; Kubli, 2003). Scattered among MCs in the distal tip of the gland are roughly 40 secondary cells (SCs). SCs are unusually large, vacuole-filled cells, ∼25 µm in diameter, whose cell biology remains relatively uncharacterized (Rylett et al., 2007; Leiblich et al., 2012). SCs have an important modulatory influence on the maintenance of postmating female responses (Minami et al., 2012; Gligorov et al., 2013). One aspect of this, reduced receptivity to remating, is regulated by SC-specific bone morphogenetic protein (BMP) signaling (Leiblich et al., 2012) via an unknown mechanism.

Exosomes are secreted membrane-bound, nanosized (40–100 nm) vesicles generated in late endosomal multivesicular bodies (MVBs; Raposo and Stoorvogel, 2013; Christianson et al., 2014). They are thought to mediate short- and long-range intercellular signaling events in biological contexts, such as immune (Théry et al., 2009) and tumor cell signaling (Ge et al.,

D.C.I. Goberdhan and C. Wilson contributed equally to this paper.

Correspondence to Clive Wilson: clive.wilson@dpag.ox.ac.uk

Abbreviations used in this paper: AG, accessory gland; ANCE, angiotensin-converting enzyme I; BMP, bone morphogenetic protein; ESCRT, endosomal sorting complex required for transport; Evi, Evenness Interrupted; iLE, immature late endosome; ILV, intraluminal vesicle; MC, main cell; mMVBL, maturing MVB or lysosome; MVB, multivesicular body; SC, secondary cell; SP, sex peptide; SV, secretory vacuole; UAS, upstream activating sequence.

Supplemental material can be found at:
http://doi.org/10.1083/jcb.201401072

The Rockefeller University Press $30.00
J. Cell Biol. Vol. 206 No. 5 671–688
www.jcb.org/cgi/doi/10.1083/jcb.201401072

2012; Azmi et al., 2013). Exosomes can carry ligands, receptors, intracellular signaling molecules, lipids, and nucleic acids, allowing them to participate in a wide range of functions at the cell surface or when their contents are discharged into target cells through fusion or endocytosis (Raposo and Stoorvogel, 2013; Christianson et al., 2014). They are probably secreted into the extracellular milieu by all cells and enter body fluids, such as plasma and urine (Nilsson et al., 2009; Lance et al., 2011; Properzi et al., 2013; Record et al., 2014).

Prostate-derived exosomes (or prostasomes) have reported functions in healthy and tumorigenic prostate (Ronquist, 2012; Soekmadji et al., 2013). In vitro studies suggest roles for prostasomes and epididymis-derived exosomes (epididymosomes) in promoting motility during sperm capacitation (Palmerini et al., 1999; Park et al., 2011; Aalberts et al., 2013) and maturation (Sullivan and Saez, 2013), respectively. In these ex vivo experiments, prostasomes fuse specifically to the head/neck region of sperm, potentially under pH control (Arienti et al., 1997; Park et. al., 2011; Aalberts et al., 2013).

Here, we demonstrate that SCs of the AG secrete exosomes in vivo. The very large size of SC endolysosomal compartments allows aspects of exosome biogenesis to be visualized in living tissue for the first time, revealing remarkably dynamic membrane deformation and fusion events. Secreted exosomes fuse with sperm in vivo in females after mating, phenocopying reported properties of human prostasomes in vitro (Arienti et al., 1997; Park et al., 2011). Furthermore, SC-derived exosomes interact with epithelial cells in the female reproductive tract and are required to induce changes in female remating behavior controlled by BMP signaling. Secretion, but not formation, of SC-derived exosomes requires BMP signaling, highlighting endolysosomal trafficking as a key regulator of SC function. Thus, regulated secretion of exosomes in the AG provides an essential part of the armory promoting male-specific interests during *Drosophila* reproduction.

Results

SCs secrete CD63-GFP–marked puncta into the AG lumen

Each AG secretes into a large lumen, which opens at its proximal end into the ejaculatory duct (Fig. 1, A–C). We expressed a GFP-tagged tetraspanin, CD63, a mammalian transmembrane exosome marker used previously to mark fly exosomes (Panáková et al., 2005; Gross, et al., 2012), independently in MCs and SCs (Figs. 1, A–C; and S1, A and B) using the GAL4/upstream activating sequence (UAS) system (Brand and Perrimon, 1993). In SCs of 3-d-old males, CD63-GFP localized to the limiting membrane of all large (>2-µm diameter) vacuoles and, in some cells, to the apical plasma membrane (Fig. 1 F). Not all vacuoles were identical, however; the majority appeared to be compartments previously described as secretory vacuoles (SVs; Rylett et al., 2007) because they had a dense core containing the secreted protease angiotensin-converting enzyme I (ANCE; Fig. 1, E and F). CD63-GFP–positive puncta, presumably representing intraluminal vesicles (ILVs), were also observed inside many vacuoles, especially in live specimens. These puncta were typically most prominent in at least one acidic compartment, stained with the vital acid-sensitive dye LysoTracker red (Fig. 1, G and H).

The AG lumen contained GFP-marked puncta (Figs. 1, C and D; and S1, A and F), which were not observed when CD63-GFP was expressed in the large number of MCs in the AG (Fig. S1 B), suggesting that only SCs secrete this tagged membrane protein. Overexpressed cytoplasmic GFP was sometimes incorporated into puncta inside SC vacuoles (Fig. S1 C), indicating that the puncta are not induced by CD63-GFP expression. Furthermore, another tagged, nonexosomal membrane protein, CD8-RFP, which labels all vacuolar compartments and is internalized in some of them, was not secreted (Fig. S1, D and E), suggesting that CD63-GFP is packaged into intraluminal structures and selectively secreted. In support of this, luminal vesicles ∼40 nm in diameter, as well as other particulate material, were observed by transmission EM in the AG lumen of wild-type males (Fig. S2 G).

CD63-GFP–positive puncta are located inside late endosomes and lysosomes

We analyzed the large SC compartments in more detail using LysoTracker red–stained living glands. Counting vacuoles by scanning through multiple focal planes revealed remarkably consistent numbers of large (>2 µm) and small (<2 µm) CD63-positive acidic compartments and large nonacidic CD63-positive compartments in each SC of 6-d-old adults (Fig. 1 I). Both classes of acidic compartments were also visible in non–CD63-GFP–expressing SCs (Figs. S1, G versus H; and 2, A–C) and therefore were not induced by CD63-GFP expression. We hypothesized that the smaller apical acidic compartments were immature late endosomes (iLEs; CD63-GFP$^+$/LysoTracker$^+$ and <2 µm; Fig. 1 I), and the large acidic compartments, at least one of which contained small CD63-GFP–positive puncta, were unusually large (≤10 µm in 6-d-old SCs) maturing MVBs or lysosomes (mMVBLs; CD63-GFP$^+$/LysoTracker$^+$ and >2 µm; Fig. 1 I). In addition, some, but not all, nonacidic SV compartments (CD63-GFP$^+$/Lysotracker$^-$ and >2 µm; Fig. 1 I) contained larger CD63-GFP–positive intraluminal structures.

In each SC, an anti-CD63 antibody, which cross-reacted with fluorescent GFP puncta in the AG lumen (Fig. S2, B and C), also stained most of the lumen of either one or two compartments, which contained only sporadic fluorescent GFP puncta (Fig. S2 A). These compartments were ANCE negative and therefore not SVs. We reasoned that they were acidic compartments in which the microenvironment must partially inhibit fluorescence of internalized GFP. To confirm that SCs have giant vesicle-containing compartments, we analyzed SC ultrastructure by transmission EM (Fig. S2, E–I). In addition to the SV compartments previously reported by Rylett et al. (2007), SCs possessed one or two less electron-dense compartments containing vesicles ∼40 nm in diameter, an appropriate size to be precursors of secreted exosomes (Fig. S2 I). The ultrastructure of these large compartments was difficult to preserve in fixed, sectioned material, but because they are not filament- and ANCE core-containing SVs, we conclude that they must represent the acidic vesicle-containing compartments we observe in live specimens.

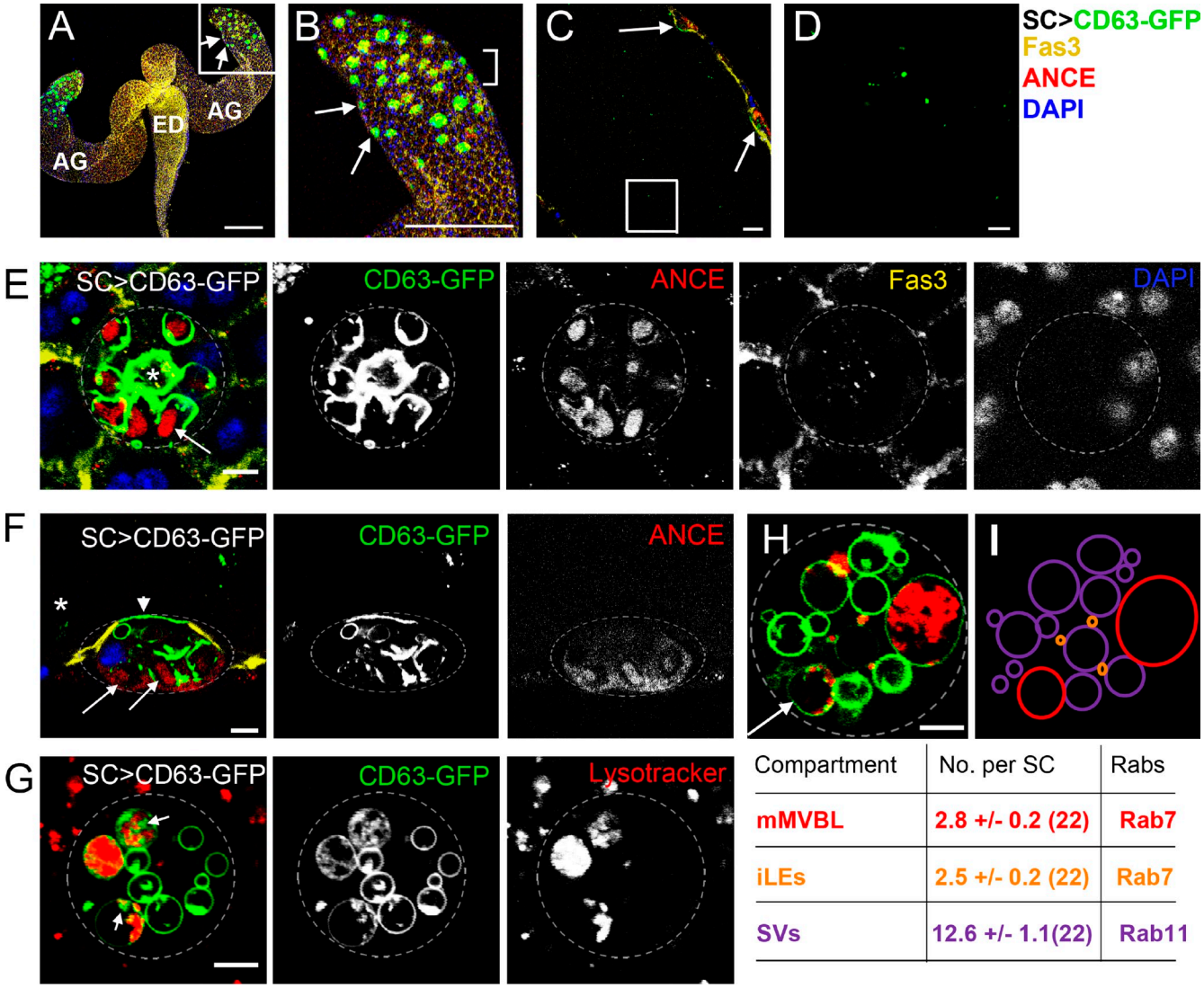

Compartment	No. per SC	Rabs
mMVBL	2.8 +/- 0.2 (22)	Rab7
iLEs	2.5 +/- 0.2 (22)	Rab7
SVs	12.6 +/- 1.1(22)	Rab11

Figure 1. **SCs secrete CD63-GFP–positive, exosome-like puncta.** (A–D) Paired accessory glands (AG) expressing CD63-GFP in SCs connect to the ejaculatory duct (ED; A). Images of different magnifications show surface sections of SCs within the AG epithelium (B; from square in A, arrows mark two SCs), a transverse section through the lumen (C; bracketed region in B, arrows mark two SCs), and CD63-GFP–positive puncta in the lumen (D; square in C; an image at higher confocal gain setting is shown in Fig. S1 F). (E and F) High magnification images of surface (E) and transverse (F; asterisk marks the lumen containing GFP puncta) sections through the SC show that CD63-GFP is also found at the apical plasma membrane (arrowhead; F) and the limiting membrane of SC vacuoles, the majority of which have a dense ANCE-positive core (highlighted with arrows). One or two CD63-GFP–lined compartments per SC lack an ANCE-stained core but contain fluorescent puncta (E, asterisk). Fasciclin3 (Fas3) marks septate junctions at the cell surface, and DAPI marks nuclei (note that SCs and MCs are binucleate). (G and H) Vital staining of SCs with LysoTracker red reveals CD63-GFP–positive puncta (putative ILVs; arrows) in large acidic compartments (mMVBLs), distinguishing them from other compartment classes, such as the more abundant secretory vacuoles (SVs) and immature late endosomes (iLEs). All images show SCs from 3-d-old males incubated at 28.5°C after eclosion. (I) Schematic representation of compartments within SC in H; values below indicate the mean total numbers of each compartment in 6-d-old control SCs counted from multiple sections along the apical–basal axis; the numbers of SCs analyzed are given in brackets. Approximate outline of the SC is marked in E–H. Bars: (A and B) 200 nm; (C) 20 µm; (D–H) 5 µm.

We performed more detailed live-imaging analysis of these large acidic and nonacidic SC compartments to confirm their identity, using selected ubiquitously expressed YFP-tagged Rab GTPases (Marois et al., 2006) that regulate endocytic trafficking and exosome secretion (Savina et al., 2002; Fader et al., 2005; Stenmark, 2009; Koles et al., 2012; Beckett et al., 2013). SCs typically contained two or three large vacuoles lined with Rab7-YFP, most of which were acidic (Fig. 2 A). Importantly, because all large acidic compartments were Rab7 positive ($n > 50$ cells), this confirms that the acidic compartments with CD63-GFP–positive puncta are either MVBs or lysosomes containing undegraded GFP. In support of this, these large acidic compartments were also lined by a GFP fusion with type II phosphatidylinositol kinase (PI4KII-GFP; Fig. S2 D), which marks late endosomes and lysosomes in other *Drosophila* secretory cells (Burgess et al., 2012).

Rab11-YFP, a marker for exocytic and recycling endocytic membranes, which regulates exosome secretion in flies (Chen et al., 1998; Koles et al., 2012; Beckett et al., 2013), localized to the limiting membrane of nonacidic SVs (Fig. 2 B). However, expression of this marker induced loss of large mMVBLs in most SCs (10/13 cells); overexpression of wild-type Rab11 therefore

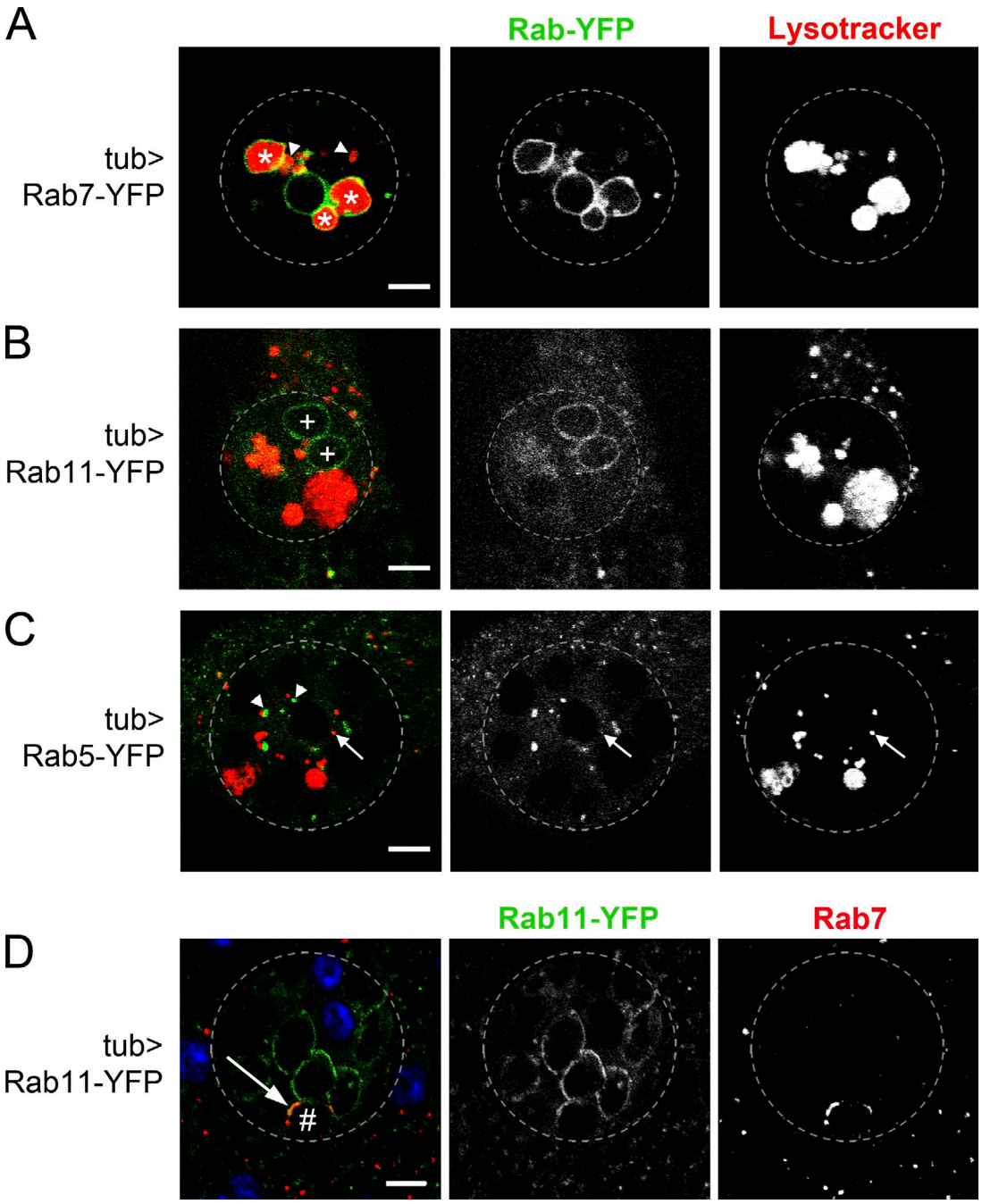

Figure 2. **Rab GTPase signatures define different SC subcellular compartments.** (A–D) SCs from 3-d-old males expressing different Rab-YFP constructs and stained with LysoTracker red. SCs have 5–10 small acidic Rab7-YFP–positive iLEs (A, arrowheads; most of these are usually located more apically than this confocal section; see Fig. 3) and 2.4 ± 0.9 (n = 11) Rab7-YFP–positive large vacuoles, 85% of which are acidic mMVBLs (A, asterisks; similar numbers [2.9 ± 0.5, n = 9] of large acidic compartments are seen in CD63-GFP–expressing SCs at this stage). Other Rab-YFP lines reveal Rab11-YFP–positive, nonacidic SVs (B, +; and D), many Rab5-YFP–positive small nonacidic compartments (C, arrowheads), and more rarely (4/16 SCs), a Rab5-YFP–positive small acidic compartment (C, arrows). In some fixed tub>Rab11-YFP SCs stained for Rab7, Rab7 colocalizes with Rab11-YFP in parts of the limiting membrane (D, arrow) of a single SV (D, #). DAPI stains nuclei (blue). Approximate outline of SC is marked in all images. Bars, 5 µm.

alters trafficking to mMVBLs, as has been found in other systems (Savina et al., 2002, 2005). Finally, Rab5-YFP, a marker for early endosomes, mainly localized to many small (<2 µm) nonacidic, centrally clustered compartments, often in close proximity to iLEs (Fig. 2 C). Interestingly, large nonacidic Rab7-YFP–positive vacuoles were typically in contact with acidic Rab7-YFP–positive iLEs (Fig. 2 A), consistent with a model in which the former compartments might derive from Rab11-positive vacuoles by fusion with iLEs. In support of this, we found Rab7 colocalizes with Rab11-YFP at the limiting membrane of a subpopulation of Rab11-YFP–lined SVs (Fig. 2 D). In conclusion, SCs contain unusually large secretory and acidic vacuoles, permitting the in vivo analysis of these compartments at high spatial resolution. At least one large acidic compartment in each SC contains CD63-positive puncta (Fig. 1, G and H), and equivalent large vesicle–containing structures are also observed by EM (Fig. S2).

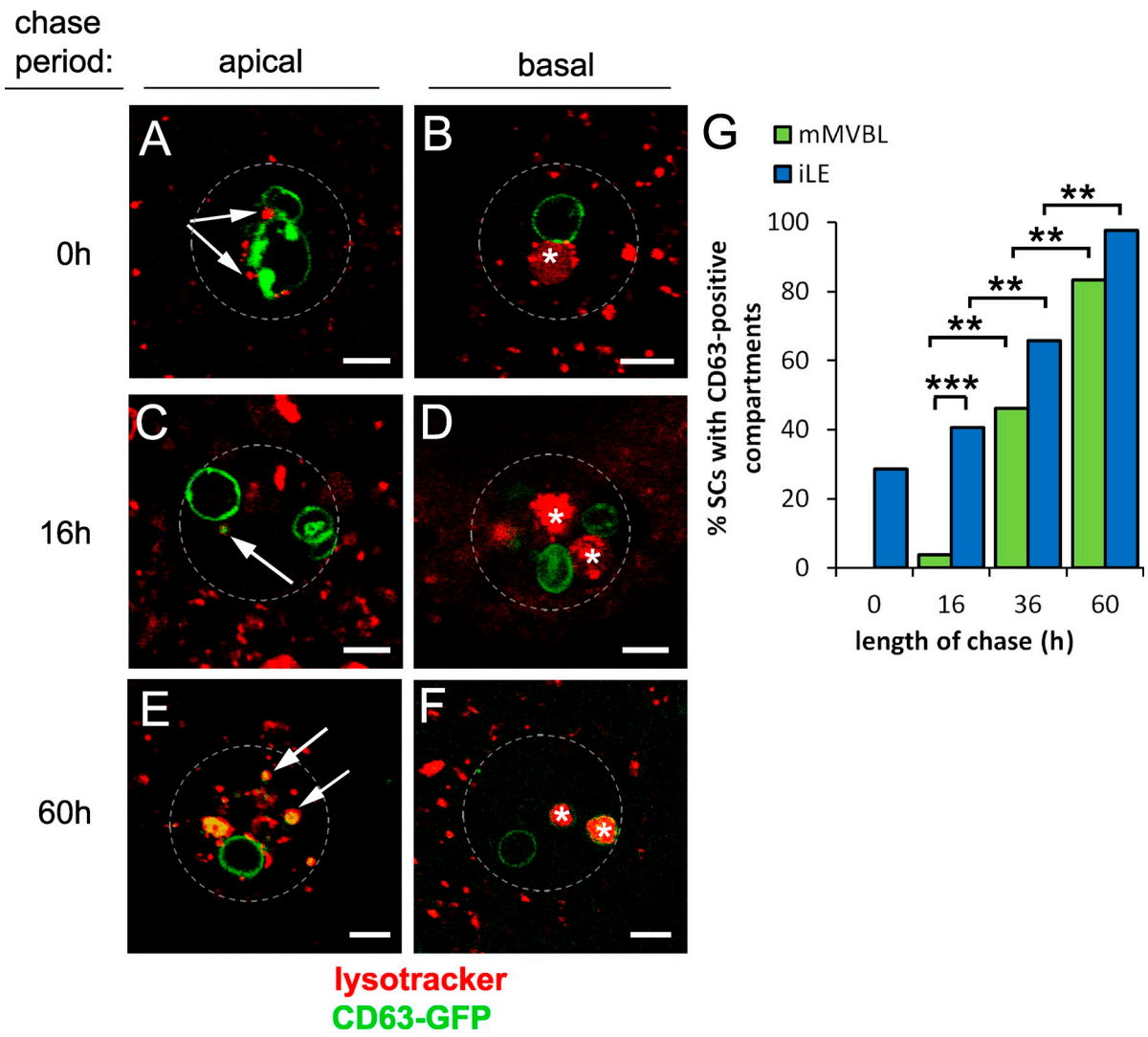

Figure 3. **CD63-GFP traffics from secretory to endocytic compartments in SCs.** (A–G) An 8-h pulse (at 28.5°C) of CD63-GFP expression was chased at 18°C for 0–60 h in virgin males, and proportions of cells with one or more LysoTracker red–positive iLEs (arrows in A, C, and E in apical sections; GFP positive in C and E) and mMVBLs (asterisks in B, D, and F in more basal views) that were CD63-GFP–positive were scored (G). Data shown are from a single representative experiment out of two repeats. The images in A–F are shown again in Fig. S3 alongside the corresponding single color channel images. Approximate outline of SC is marked in all images. **, $P < 0.01$; ***, $P < 0.001$; $n > 24$, pairwise comparisons, Fisher's exact test. Bars, 5 µm.

Endolysosomal and secretory compartments in SCs are highly dynamic

We followed CD63-GFP trafficking through the secretory and endolysosomal systems using a pulse–chase approach. Induction of a short (8 h) pulse of CD63-GFP expression, by inhibiting the temperature-sensitive GAL4 transcriptional repressor GAL80^{ts} at 28.5°C, followed by a chase period at 18°C of 0–60 h, revealed rapid labeling of two (1.9 ± 0.2, $n = 17$) nonacidic SVs, presumably receiving newly synthesized CD63-GFP from the Golgi (Figs. 3, A and B; and S3, A and B). Some iLEs were also GFP positive immediately after the pulse. During the early part of the time course, a greater proportion of SCs contained labeled iLEs than labeled mMVBLs ($P = 0.001$, $n > 27$), and this trend continued at later time points (Figs. 3, A–G; and S3, A–F), supporting our model in which CD63-GFP traffics first to the iLEs and subsequently to mMVBLs.

Strikingly, real-time confocal imaging of SCs revealed nonacidic SVs fusing with mMVBLs and rapid exchange of limiting membrane components (Fig. 4 A and Video 1). Although the internal contents of these compartments did not mix freely, these findings suggest a surprising level of exchange between SVs and mMVBLs and might explain how CD63-GFP–positive structures accumulate in SVs (Fig. 1, E–H).

As discussed previously, anti-CD63 staining indicates that GFP in many CD63-positive ILVs does not fluoresce (Fig. S2 A). However, inward invaginations of the CD63-GFP–labeled limiting membrane into the mMVBL lumen were observed in time-lapse videos, and occasionally, it appeared that new fluorescent ILVs might be formed from these (Fig. 4 B and Video 2). Therefore, some steps in ILV formation can be visualized by confocal microscopy in the large mMVBLs of living SCs, allowing us to screen for genetic manipulations that block these processes.

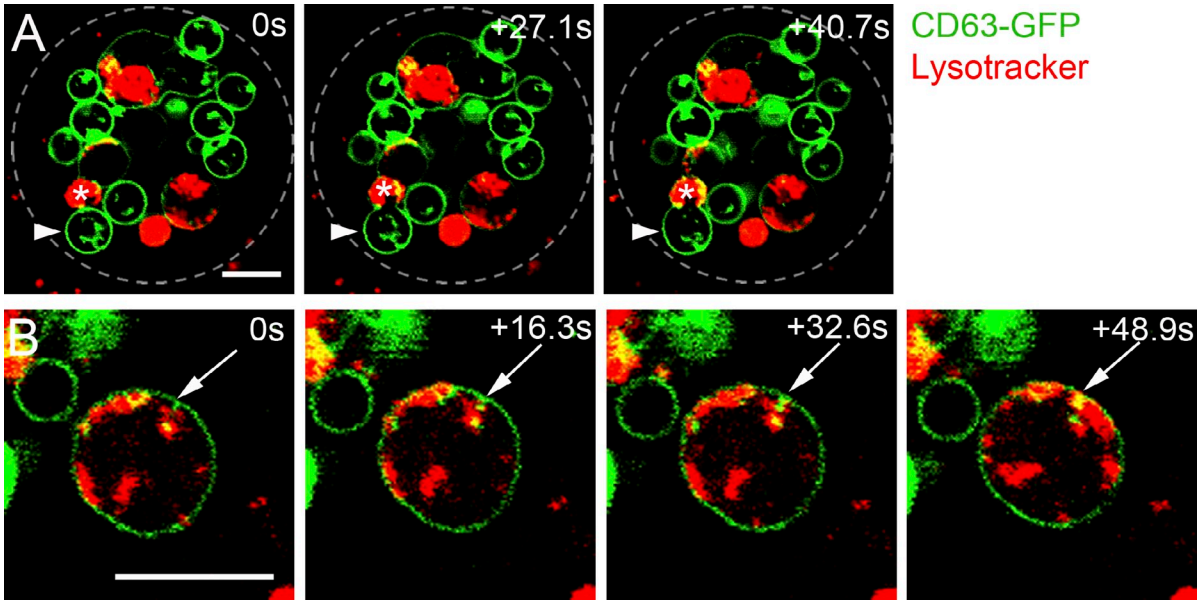

Figure 4. **Real-time imaging reveals dynamic endolysosomal trafficking events.** (A and B) Time-lapse imaging of 3-d-old *SC>CD63-GFP* males stained with LysoTracker red. (A) An mMVBL containing ILVs (asterisks) fuses with a large nonacidic SV (arrowheads; Video 1). Approximate outline of SC is marked. (B) A CD63-GFP–marked protrusion invaginates from the mMVBL membrane (arrows; 0 s) and seems to form a CD63-GFP–positive punctum in the next frame. Later, a line of peripheral acidic microdomains is seen below (48.9 s; see also Video 2). Bars, 5 µm.

Endosomal sorting complex required for transport (ESCRT)-dependent secretion of exosomes in SCs

To assess whether CD63-GFP–positive puncta in the AG lumen are exosomes derived from mMVBLs of SCs, we specifically blocked expression or function of a broad range of molecules in SCs, which in other systems are implicated in exosome biogenesis. The ESCRT complex has well-characterized roles in ILV formation, although ESCRT-independent mechanisms have also been reported (Trajkovic et al., 2008). Hrs is a component of the ESCRT-0 complex directly involved in protein sorting into ILVs and ILV formation through subsequent recruitment of downstream ESCRTs (Lloyd et al., 2002; Katzmann et al., 2003). Several recent studies demonstrate a role for Hrs in ESCRT-dependent exosome secretion in mammals and flies (Tamai et al., 2010; Gross et al., 2012; Colombo et al., 2013). ALiX (ALG-2–interacting protein X) interacts with several ESCRT complex proteins (Matsuo et al., 2004; Odorizzi, 2006). Recent knockdown studies in mammalian cells indicate that it is required in exosome biogenesis (Matsuo et al., 2004; Baietti et al., 2012), but this has not been investigated in flies. Fluorescent ILVs inside mMVBLs were almost completely absent in SCs expressing either *Hrs-RNAi* or *ALiX-RNAi* constructs, unlike controls (Fig. 5, B–D). The number of CD63-GFP–positive puncta secreted into the AG lumen was also drastically reduced ($P < 0.001$, $n > 9$; Fig. 5 A). mMVBLs in *ALiX-RNAi*– and *Hrs-RNAi*–expressing SCs were smaller and larger than controls, respectively (Fig. 5 I). These genotypes had normal numbers of iLEs (Fig. 5 H), but *Hrs-RNAi*–expressing SCs had significantly fewer mMVBLs (Fig. 5 G). Importantly, these *ESCRT* knockdown SCs still synthesized equivalent levels of the SC-specific CD63-GFP fusion protein by Western blot analysis of whole glands (Fig. 5 J) but transferred much less protein to females upon mating (Fig. 5 K), consistent with the reduced secretion of this exosome marker.

An alternative explanation for these results is that *ESCRT* knockdown affects all secretion by SCs. However, the SC-specific production (Rylett et al., 2007) of the secreted, nonexosomal protease ANCE (Figs. 5 J and S4, B–D), its secretion into the AG lumen (Fig. S4, E–G), and its transfer into females (Fig. 5 K) were not affected by *ALiX* or *Hrs* knockdown, showing that these treatments selectively affect the exosome biogenesis pathway in SCs.

To provide further evidence that SCs produce CD63-positive exosomes, we modulated the activities of three Rabs previously implicated in exosome secretion: Rab11 (Savina et al., 2002; Koles et al., 2012; Beckett et al., 2013), Rab35 (Hsu et al., 2010), and Rab27 (Ostrowski et al., 2010). Expression of dominant-negative Rab11-YFP (*Rab11DN*; Zhang et al., 2007), *Rab11-RNAi*, *Rab35-RNAi*, and one of two *Rab27-RNAi*'s significantly reduced the number of secreted GFP-positive puncta (Figs. 5 A and S5, A and B). Previous studies have indicated that Rab35 and Rab27 do not regulate secretion of exosomes carrying the cargo receptor Evenness Interrupted (Evi) in *Drosophila* S2 cells (Koles et al., 2012; Beckett et al., 2013), suggesting multiple exosome secretion routes in flies as well as mammals. Indeed, expression of two different RNAi's targeting *Evi*, which is required to produce Wingless-containing exosomes (Beckett et al., 2013) but is not required for CD63-GFP–positive exosome secretion in flies (Gross et al., 2012), did not affect the number of secreted puncta in the gland lumen (Fig. 5 A). Finally, the number of secreted puncta was also significantly reduced when *Rab7-RNAi* or dominant-negative Rab7-YFP (*Rab7DN*; Zhang et al., 2007) was expressed in SCs (Fig. 5 A), implicating late endolysosomal trafficking events in secretion. Based on these extensive genetic data,

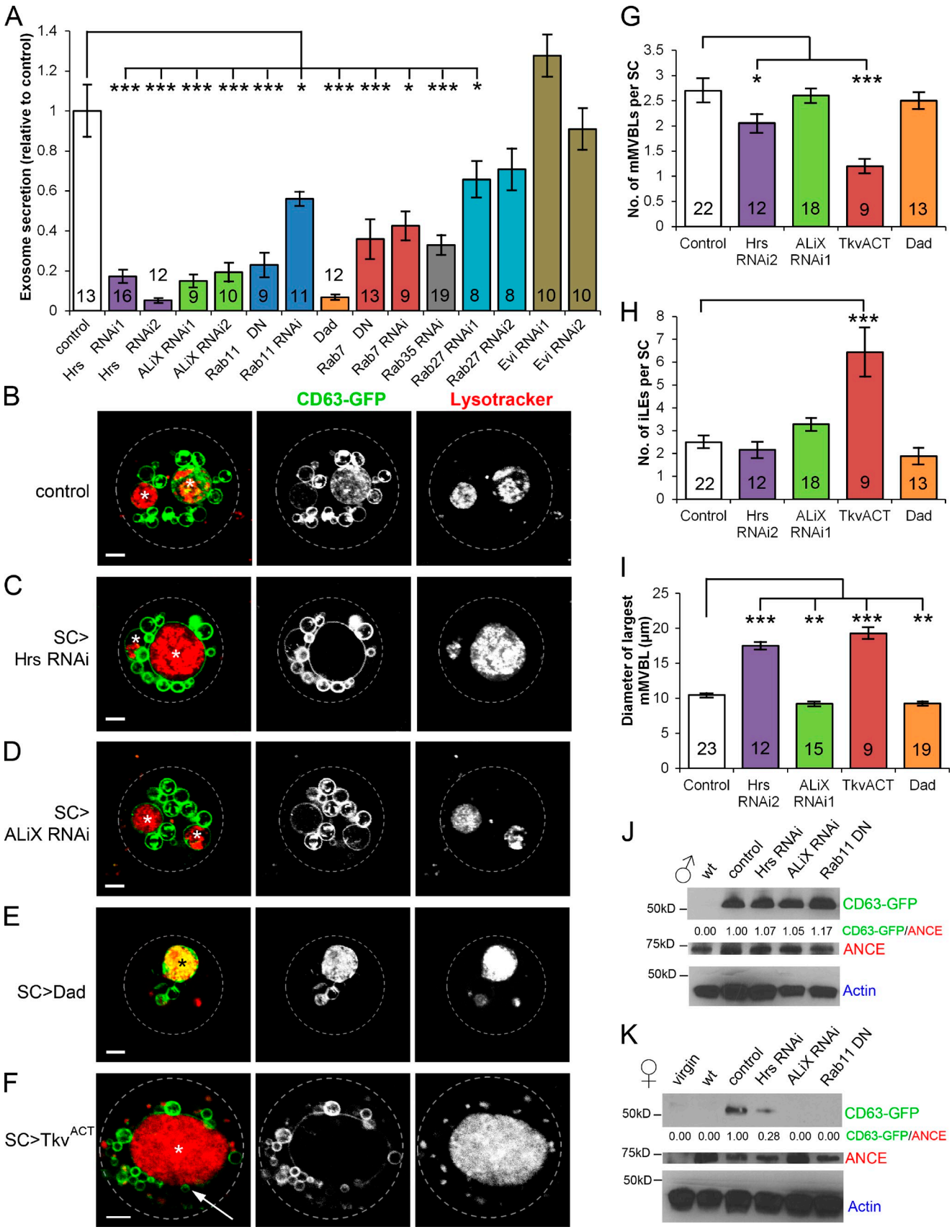

Figure 5. **ESCRTs, Rab GTPases, and BMP signaling regulate the exosome biogenesis pathway.** (A) The numbers of CD63-GFP–positive puncta secreted into the AG lumen were significantly reduced in *SC>Hrs-RNAi*, *SC>ALiX-RNAi*, *SC>Rab11DN*, *SC>Rab11-RNAi*, *SC>Dad*, *SC>Rab7-DN*, *SC>Rab7-RNAi*, *SC>Rab27-RNAi1*, and *SC>Rab35-RNAi* males compared with control (number of glands above or in the bars) but not *SC>Rab27-RNAi2* and

we conclude that SCs secrete CD63-GFP–positive exosomes whose biogenesis and secretion are regulated by evolutionarily conserved molecular mechanisms.

Interestingly, despite the large number of CD63-GFP–positive exosomes in the AG lumen, they did not seem to fuse with MCs in most of the gland (Fig. S5 C). However, we did observe occasional GFP puncta inside MC neighbors of SCs at the distal tip of each AG (Fig. S5 D). The regionalized nature of this uptake indicates that it may be mediated by contact-dependent transfer between SCs and MCs, rather than transfer via the AG lumen.

SC exosomes fuse with sperm and interact with epithelial cells in the female reproductive tract

We investigated whether the interaction between SC exosomes and target cells primarily takes place after mating. *SC>CD63-GFP* males transferred fluorescent puncta into the lumen of the female reproductive tract during mating (Fig. 6, A–D). Multiply mated males of 11 d and older can sporadically transfer SCs to females (Leiblich et al., 2012). Importantly, all mating experiments performed in our current study were with 4-d-old males; we never observed transfer of fluorescent SCs in >50 mated females that we imaged, indicating that SC transfer is not involved in the phenotypes observed.

Several seminal peptides target specific regions of the female reproductive tract and/or sperm after mating (Peng et al., 2005; Ravi Ram et al., 2005). Isolated human prostasomes fuse with the sperm midpiece in vitro, delivering Ca^{2+} signaling molecules implicated in sperm motility (Fabiani et al., 1994; Park et al., 2011). We also detected colocalization of CD63-GFP and sperm heads in the female reproductive tract after mating (Fig. 6, D and E). Analysis of confocal z series images revealed narrow rings of GFP surrounding the sperm head (Fig. 6 F), as might be expected after exosome–sperm fusion. These events were most commonly observed at 20 min after the start of mating (88% [14/16] mated females; Fig. 6 H) in the anterior portion of the female reproductive tract where sperm and exosomes accumulated, either in the anterior uterus (9/16) or the oviduct (5/16). This fusion frequency is almost certainly underestimated: first, because CD63-GFP is likely to rapidly diffuse and dissipate over the sperm surface after fusion, so the GFP fluorescence signal will rapidly become undetectable, and second, because there may be additional fusion to sperm tails. Although tools were not available to fluorescently colabel exosomes and sperm tails, pairs of short parallel fluorescent lines or extended irregular lines of GFP fluorescence were always seen in the female reproductive tract lumen (100%, $n = 8$; Fig. 6, F and G; and Video 3), which might represent such events. We did not observe CD63-GFP in sperm storage organs, though as discussed previously in this paper, GFP may dissipate after fusion to sperm before entering these structures.

Interestingly, we noted accumulation of CD63-GFP exosomes at the surface of the reproductive tract either in the uterus or oviduct in 40% of females (Fig. 7; $n = 34$), suggesting that SC exosomes also interact with female epithelial cells. In some cases, fluorescent aggregates made contact with the epithelium (Fig. 7 C and Video 4), whereas in others, dispersed puncta aligned along the epithelial surface (Fig. 7 D). These interactions may reflect docking to female cell targets, either before internalization via endocytosis (Morelli et al., 2004) or possibly as part of a cell surface signaling mechanism. In summary, SC-derived exosomes do not seem to fuse to the AG epithelium in virgin males but do fuse to sperm and interact with female epithelial cells after mating.

SC exosomes modulate female receptivity to remating

In contrast to virgin females, recently mated *Drosophila* females will reject a courting male (Wolfner, 1997). We have previously shown that BMP signaling in SCs is required for full induction of this female postmating behavior (Leiblich et al., 2012). We hypothesized that SC-derived exosomes might be involved in this function. Remarkably, blocking exosome production, using SC-specific expression of either *ALiX-RNAi* or dominant-negative Rab11, reduced the ability of males to prevent female remating (Fig. 8 A). Importantly, and similar to our observations when BMP signaling is blocked in SCs (Leiblich et al., 2012), we did not see any significant effect on egg laying, fecundity, or mating behavior for *SC>ALiX-RNAi* males (mating times, but not egg laying or fecundity, were reduced for *Rab11DN*; Fig. 8, B–F). Therefore, exosome secretion from SCs appears to be required to fully induce long-term postmating reprogramming of female behavior.

BMP signaling regulates endolysosomal trafficking and is required for exosome secretion

Blocking SC function and development affects multiple aspects of fecundity (Minami et al., 2012, Gligorov et al., 2013), but reduced BMP signaling and loss of exosome secretion in

SC>Evi-RNAi males. DN, dominant negative. (B–F) SCs from 6-d-old virgin males stained with LysoTracker red. (G–I) Different intracellular compartments were subsequently counted and measured. mMVBLs (asterisks) in SCs expressing CD63-GFP and *Hrs-RNAi* (C) or *ALiX-RNAi* (D) contain very few CD63-GFP–positive ILVs (internal puncta), unlike controls (B), and are altered in size (I). Reducing levels of BMP signaling in SCs (Dad overexpression; E) results in significantly smaller mMVBLs (I), typically containing a higher density of internalized fluorescent CD63-GFP than controls. SCs expressing an activated form of the BMP receptor Tkv^{ACT} (F) contain fewer mMVBLs (G), which are larger (I), and typically surrounded by multiple SVs (e.g., arrow). They also contain more iLEs (H). (G–I) Mean number of mMVBLs (G) and iLEs (H) and mean diameter of largest mMVBL (I) in SCs of different genotypes (I). Quantification in G–I is from a mean of three cells per gland, averaged over *n* glands (numbers in bars). (J) Western analysis of AG protein extracts from w^{1118} (wild type [wt]) and flies expressing *SC>CD63-GFP* with or without (control) different transgenes. (K) Western analysis of protein extracts from reproductive tracts dissected from females mated to males of the same genotypes. CD63-GFP/ANCE is the ratio of signals from Western blots. Full-length CD63-GFP protein is observed in males and females. Error bars indicate ±SE; *, $P < 0.05$; **, $P < 0.01$; ***, $P < 0.001$ relative to control. Data were analyzed using either an unpaired two-tailed Student's *t* test or Mann–Whitney *U* test, for normally and nonnormally distributed datasets, respectively. Approximate outline of SC is marked. Bars, 5 µm.

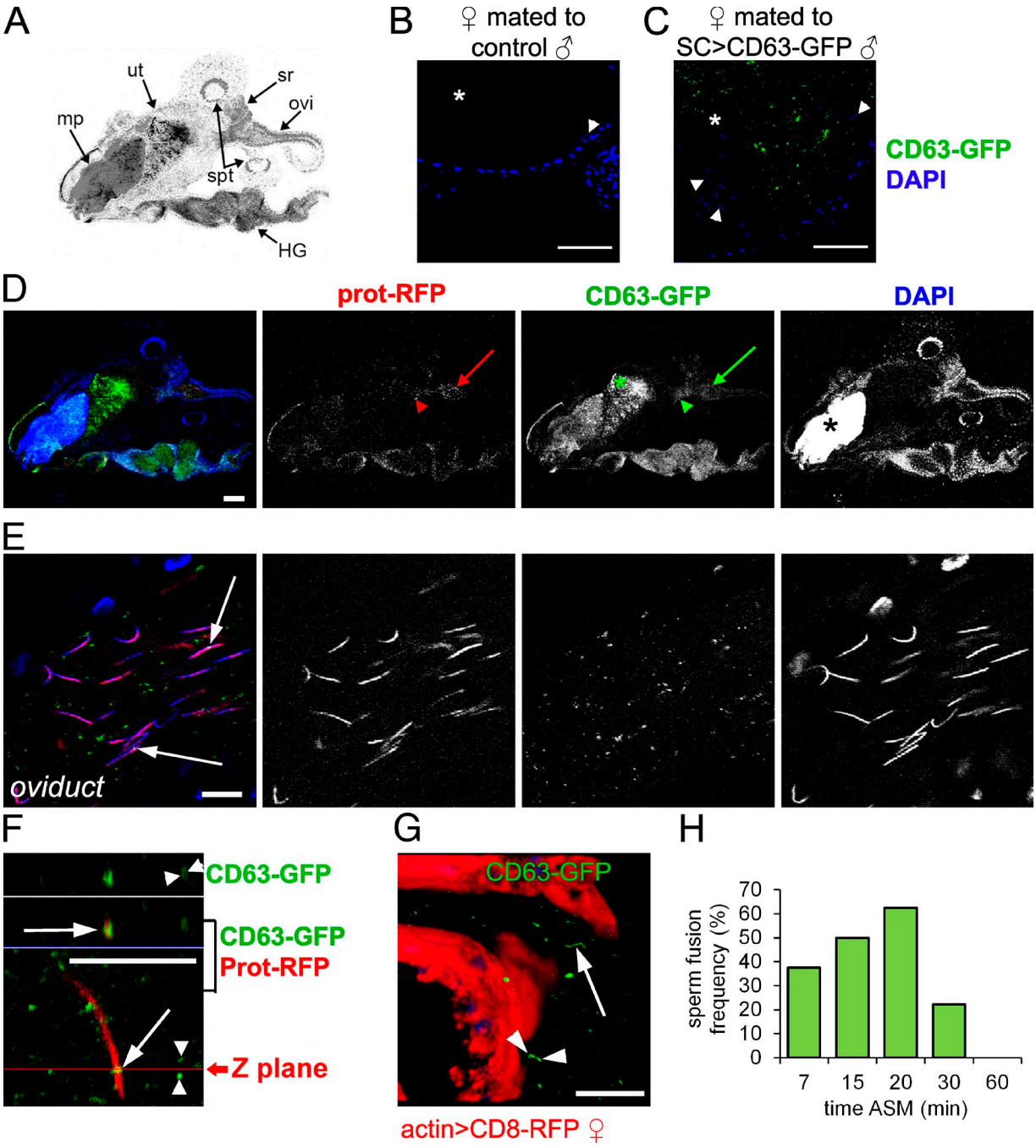

Figure 6. **SC exosomes interact with sperm in females.** (A) Schematic of female reproductive tract in D showing mating plug (mp), uterus (ut), oviduct (ovi), and sperm storage organs (spermathecae [spt] and seminal receptacle [sr]) as well as the autofluorescent hindgut (HG). (B and C) w^{1118} female reproductive tract dissected 20 min after mating to either a control w^{1118} (B) or *SC>CD63-GFP* (C) male, imaged under identical confocal settings. Images show lumen of the female uterus (asterisks) containing sperm whose heads are visible with DAPI staining (arrowheads). (D and E) Female reproductive tracts 20 min after mating to a *protamineB-RFP; SC>CD63-GFP* male. (D) ProtamineB-RFP (prot-RFP), which marks sperm heads, accumulates in the anterior uterus (red arrowhead) and oviduct (red arrow). Most CD63-GFP–positive exosomes localize to the posterior uterus (green asterisk), but they can also be seen in the anterior uterus (green arrowhead) and oviduct (green arrow). The autofluorescent mating plug (closed asterisk) is shown. (E) CD63-GFP–positive exosomes colocalize with sperm heads marked by protamineB-RFP (open arrows). (F) Orthogonal view of a z stack through near-complete ring of CD63-GFP fused to ProtamineB-RFP sperm head (arrows). The confocal image below the blue line shows part of the female reproductive tract lumen. The two images above the blue line, separated by a white line, are green (top) and red/green (bottom) z stacks captured in the z plane marked in the bottom image. Note multiple pairs of parallel GFP-positive lines (arrowheads), potentially produced by sperm tail fusion. (G) These (arrowheads) and irregular extended lines of fluorescence (arrow) are also seen in G, which shows a maximum 3D projection image of a z stack from a female anterior uterus and oviduct where the epithelium is marked by actin>CD8-RFP (also shown in Video 3). (H) Female reproductive tracts were dissected and fixed at specific times after the start of mating to *SC>CD63-GFP* males. The frequency of exosome–sperm interaction events within the female reproductive tract was analyzed (n = 8 for each time point after the start of mating [ASM]). Only fusions to the sperm heads are included. Bars: (B and C) 50 µm; (D) 200 µm; (E and F) 5 µm; (G) 20 µm.

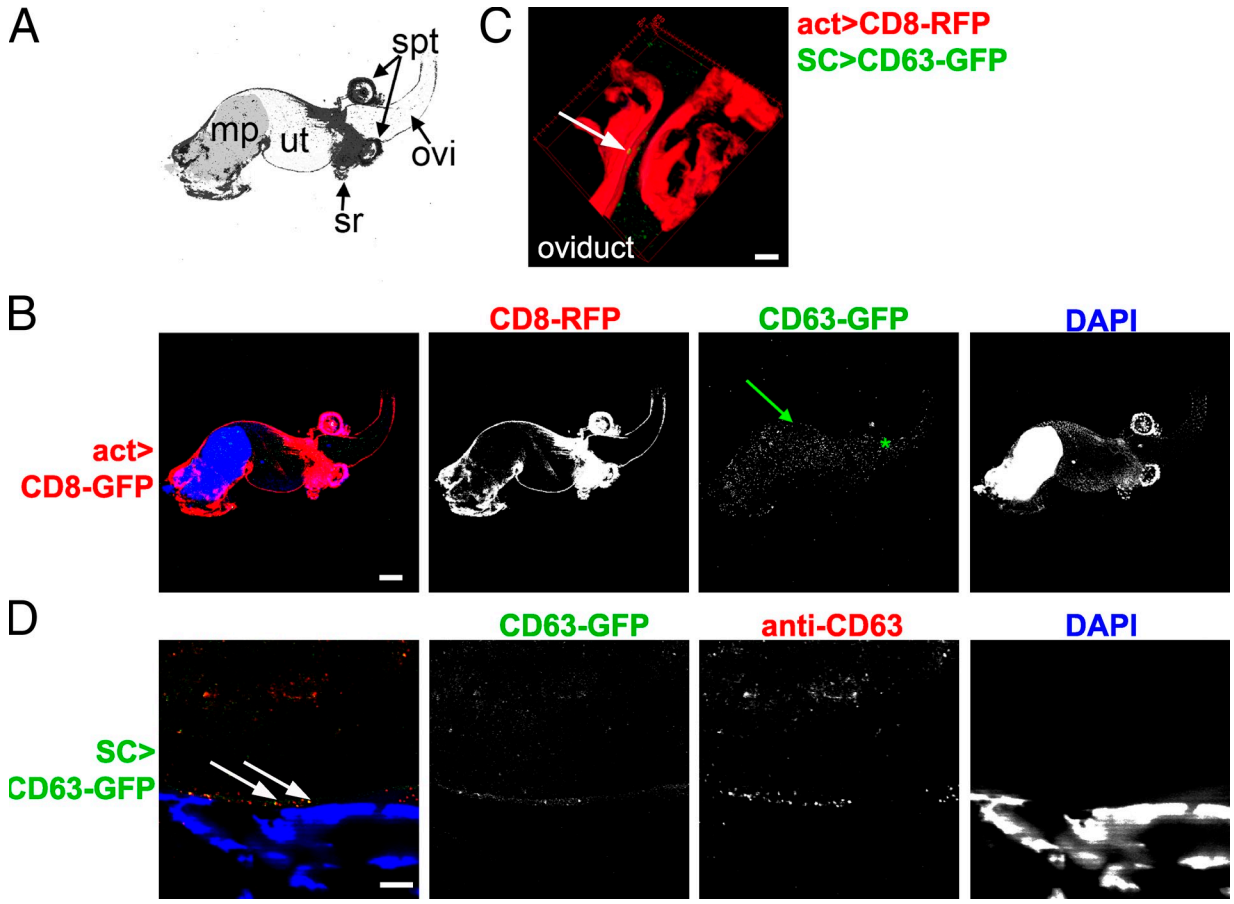

Figure 7. **SC exosomes interact with female epithelial cells.** (A) Schematic of female reproductive tract shown in B. mp, posterior mating plug (autofluorescent); ut, uterus; sr, seminal receptacle; spt, spermathecae; ovi, oviduct. (B–D) *actin>CD8-RFP*–expressing (B and C) or wild-type (D) females mated to *SC>CD63-GFP* males. (B) CD63-GFP exosomes are found in the uterus (green arrow) and oviduct (green asterisk). (C and D) These exosomes accumulate at the apical surface of female reproductive tract epithelial cells (arrows), which are either marked with CD8-RFP (C; Video 4) or unmarked (D). DAPI stains nuclei. In D, the reproductive tract is stained with an antibody against human CD63 to confirm that GFP and CD63 colocalize. Specific spermathecal cells exhibit weak autofluorescence. Bars: (B) 200 µm; (C) 20 µm; (D) 5 µm.

these cells specifically modulate female remating behavior. One possible explanation is that BMP signaling controls exosome production. Remarkably, antagonizing BMP signaling by expression of the negative regulator Dad almost completely blocked CD63-GFP–labeled exosome secretion (Fig. 5 A), strongly supporting this idea. Unfortunately, it was not possible to test the effect of elevated BMP signaling on exosome secretion by expression of a constitutively activated form of the BMP type I receptor Thickveins (Tkv^{ACT}, containing a Q199D substitution; Hoodless et al., 1996). The hypertrophic SCs induced by expression of this construct protrude into the AG lumen and shed large amounts of GFP-positive cellular debris (Leiblich et al., 2012), interfering with exosome counting.

We tested whether BMP signaling might modulate exosome secretion by altering endolysosomal trafficking in SCs, using live imaging of CD63-GFP–expressing cells. In contrast to the effect of *ALiX* and *Hrs* knockdown (Fig. 5, C and D), mMVBLs in *Dad*-expressing SCs contained unusually high levels of internalized CD63-GFP (Fig. 5 D), indicating that BMP signaling is not required for ILV formation but must control a key trafficking and/or maturation event from the mMVBL to the plasma membrane and lysosomes, where GFP fluorescence would be lost. Indeed, SCs overexpressing Tkv^{ACT} had significantly fewer, but much larger, mMVBLs ($P = 0.04$; Fig. 5, G and I) with no intraluminal fluorescence, supporting this model. Numbers of iLEs were elevated (Fig. 5 H), and more of these cells than control cells (17/19 versus 16/31; $P = 0.003$, Fisher's exact test) contained multiple SVs clustered around the enlarged mMVBL, consistent with the idea that there is increased bulk trafficking into the large acidic compartment. We therefore conclude that BMP signaling controls a key endolysosomal trafficking step in SCs required for exosome secretion, and this potentially explains the role of SC-specific BMP signaling in modulating female postmating behavior.

Because BMP signaling drives SC growth, as measured by relative size of SC versus neighboring MC nuclei (Leiblich et al., 2012), we tested whether exosome formation or secretion might be involved in this. Interestingly, although nuclei of SCs expressing either *ALiX-RNAi* or *Rab11DN* were reduced in size, nuclear size was increased in *Hrs-RNAi*–expressing SCs (Fig. 9). This suggests that ESCRT-dependent ILV formation is not required for SC growth.

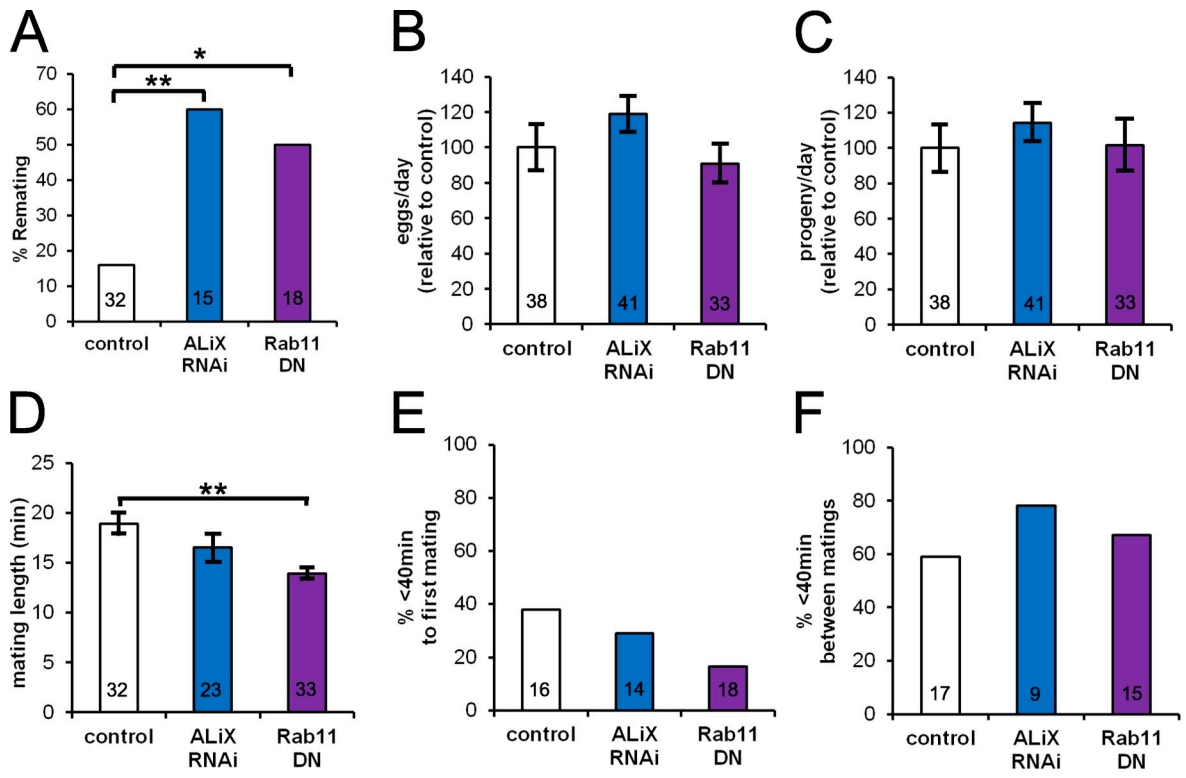

Figure 8. **Knockdown of *ALiX* in SCs selectively affects female postmating receptivity to other males.** (A) Proportion of premated 4-d-old males of different genotypes unable to prevent all females it subsequently mates with from remating (*, $P < 0.05$; **, $P < 0.01$, Fisher's exact test). (B and C) Egg counts (B) and progeny counts (C) from mated females before remating experiments were performed (analyzed by unpaired two-tailed Student's *t* test after a Shapiro–Wilk test to confirm normality). (D–F) Mating times (D; **, $P < 0.01$, Student's *t* test), proportion of males that mate within the first 40 min of exposure to females (E) or remate within 40 min of the end of previous mating (F), were also analyzed (using Fisher's exact test for E and F). Values inside bars show the number of males tested (*n*). Error bars indicate ±SE. Data shown are from a single representative experiment out of two repeats. DN, dominant negative.

Discussion

Seminal fluid synthesized by male reproductive glands has a powerful influence on fertility, affecting multiple sperm activities and altering female behavior, in some cases directly conflicting with female reproductive interests. Several previous studies have revealed an important function for seminal peptides in *Drosophila* (Chen et al., 1988; Wolfner, 1997) and mammals (Park et al., 2011; Kershaw-Young et al., 2012) in these processes. However, in this study, we present the first in vivo evidence that exosomes also play a key role and identify a completely novel role for BMP signaling in regulating this process.

SCs secrete exosomes: A new in vivo model to study exosome biogenesis

Exosome biogenesis, secretion, and uptake have been previously studied in *Drosophila* (Gross et al., 2012; Koles et al., 2012; Beckett et al., 2013). However, the small size of exosomes, MVBs, and fly tissues makes these processes difficult to analyze in vivo. The AG contains only nanoliter volumes of secretions, making it impractical to use standard exosome analysis techniques, such as ultracentrifugation and Nanosight Tracking Analysis (Vlassov et al., 2012). Like other studies in flies, we used genetic and imaging approaches to test the identity of SC-specific CD63-positive puncta. In addition, we used Western blot analysis of transferred seminal fluid and live imaging of giant MVBs in SCs to test our hypothesis that SCs produce exosomes.

We primarily used the human CD63-GFP tetraspanin marker in our analysis. However, GFP-positive puncta were also observed in large secretory compartments of SCs expressing cytosolic GFP, and exosome-sized vesicles in MVBs and the AG lumen were observed in EM analysis of wild-type glands (Fig. S2), confirming their presence in nontransgenic flies. Because exosomes can be loaded with many cellular components, our findings provide a potential explanation for the observation that AGs of several insects, including *Drosophila*, secrete intracellular proteins (Walker et al., 2006; Sirot et al., 2011).

Other evidence strongly supports the idea that CD63-positive puncta secreted from SCs are exosomes and not vesicles shed from the plasma membrane. This includes the observation that CD63-positive puncta are found inside both acidic Rab7-positive MVB-like compartments as well as nonacidic Rab11-positive vacuoles and require the ESCRT and ESCRT-associated proteins Hrs and ALiX, as well as several Rabs linked to mammalian exosome secretion, to be formed and secreted. Secreted puncta counts have been used previously in flies to study genetic control of exosome secretion (Gross et al., 2012). A criticism of this approach is that reduced puncta numbers may merely reflect aggregation. However, the transfer of CD63-GFP to females was drastically reduced in mutant backgrounds, arguing

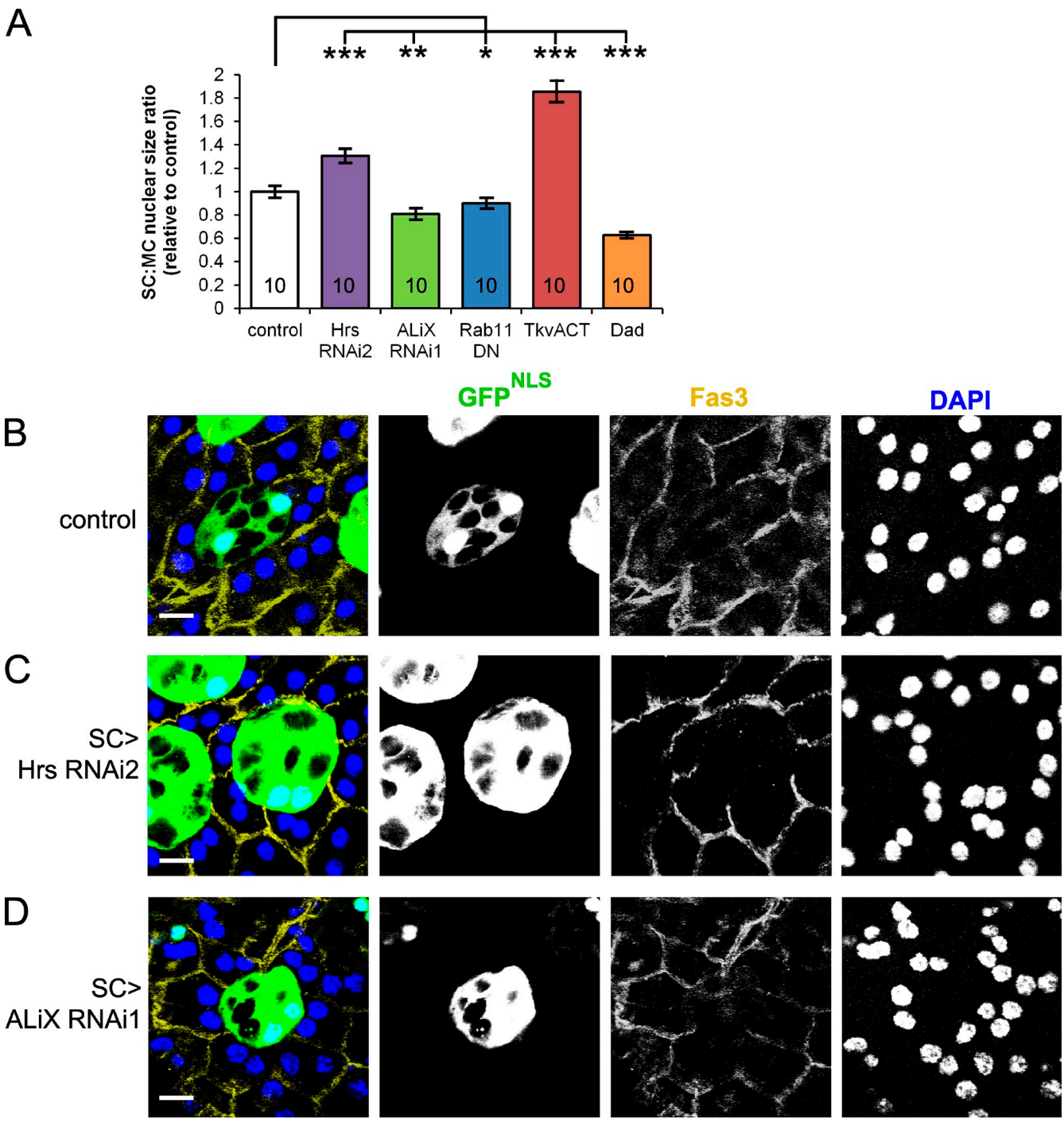

Figure 9. ***ALiX* and *Hrs* have different effects on SC growth.** (A) Growth of SCs relative to MCs in 6-d-old males expressing different transgenes in SCs, as measured by the ratio of SC to MC nuclear size and normalized to controls. Values inside bars show number of males tested (*n*). DN, dominant negative. (B–D) SCs in 6-d-old males expressing either GFP linked to a nuclear localization sequence (GFP^{NLS}) alone (B) or in combination with either *Hrs-RNAi* (C) or *ALiX-RNAi* (D), under the control of the *esgF/O*^{ts} driver. Control SC nuclei are smaller than MC nuclei at eclosion but grow to be larger by 6 d (B). Data for A were analyzed using the Student's *t* test or Mann–Whitney *U* test (*, $P < 0.05$; **, $P < 0.01$; ***, $P < 0.001$, $n = 10$) after a Shapiro–Wilk test for normality. Error bars indicate ±SE. Bars, 10 µm.

against a simple aggregation model. Furthermore, because genetic manipulation of ESCRT function does not alter other secretory processes in SCs (Figs. 5 K and S4), this strongly implicates the endocytic pathway in secretion of tagged CD63.

Studies of exosomes in *Drosophila* as well as mammals already suggest that multiple exosome subtypes exist and may be regulated differently, e.g., different roles for ALiX (Baietti et al., 2012 versus Colombo et al., 2013), Hrs (Edgar et al., 2014), and Evi (Beckett et al., 2013). If different exosome subtypes are made in SCs, these cells should offer an ideal system to study their differential regulation.

The remarkably large size of endosomal compartments in SCs provides new opportunities to study exosome biogenesis in vivo. To date, many studies of the intracellular exosome

biogenesis machinery and endolysosomal trafficking in higher eukaryotes have relied on expressing an activated form of Rab5 (Stenmark et al., 1994; Hirota et al., 2007; Wegner et al., 2010; Dores et al., 2012; Schroeder et al., 2012) or addition of the ionophore monensin (Savina et al., 2002) in cell culture to artificially enlarge the endolysosomal compartments, disrupting normal trafficking events. Hence, our new SC in vivo model should allow us to reinvestigate previously reported regulators of exosome biogenesis and identify functional differences in trafficking phenotypes, as we have seen for *Hrs* and *ALiX*.

Our study has already revealed a surprisingly dynamic interaction between the secretory and endolysosomal systems in SCs. Communication between these compartments using vesicular transport and tubulation processes has been reported in other cell types in flies and mammals (Savina et al., 2005; Minogue et al., 2006; Burgess et al., 2012), but our study suggests that direct fusion can also be involved. Indeed, our data are also consistent with mMVBLs forming after fusion between SVs and iLEs (Fig. 2 D), suggesting that fusion events may play a critical role in establishing distinct compartments within SCs. In light of this dynamic flux between compartments, it remains unclear whether CD63-GFP–labeled exosomes might be released by the classical route involving mMVBL fusion to the plasma membrane or via an intermediate secretory compartment.

SC exosomes have complex physiological functions

Although most analysis of the fly AG has highlighted roles for MC products, such as SP (Chen et al.,1988; Chapman et al., 2003), in reprogramming female postmating responses, several recent studies have also suggested a central but poorly defined function for SCs (Leiblich et al., 2012; Minami et al., 2012; Gligorov et al., 2013). A transcriptional program regulated by the *Hox* gene *Abd-B* controls vacuole formation in SCs (Gligorov et al., 2013). Our findings now indicate that at least one of the effects mediated by SCs, altered receptivity to remating, requires exosome secretion.

It is difficult to accurately estimate the frequency of SC exosome–sperm fusion events in each female fly because they can probably only be visualized transiently, and many may involve fusion to the very long sperm tail. Sperm play an essential role as mediators of SP-dependent postmating effects in females (Liu and Kubli, 2003; Peng et al., 2005), so it is plausible that exosome fusion to sperm may modulate specific SP functions. Another appealing hypothesis is that SC exosomes also interact with the female reproductive tract to influence female behavior. However, whatever the target tissues, our data clearly demonstrate a role for SC exosomes in female reprogramming. Furthermore, like human prostasomes (Arienti et al., 1997; Park et al., 2011), SC exosomes fuse with sperm, highlighting possible conserved roles for exosomes in male reproductive biology. In prostate cancer, prostasomes are inappropriately secreted into the bloodstream (Sahlén et al., 2004; Tavoosidana et al., 2011), so that other cells in the body may be subjected to these powerful reprogramming functions, potentially supporting tumor–stroma interactions and metastasis (Ronquist et al., 2010; Ge et al., 2012).

BMP-dependent regulation of endolysosomal trafficking and exosome secretion

Reducing BMP signaling in SCs inhibits exosome secretion and leads to the formation of a novel mMVBL compartment that is filled with fluorescent CD63-GFP. A simple interpretation of this result is that MVBL compartments in these cells do not mature properly, blocking exosome secretion. Consistent with this, increasing BMP signaling in these cells produces a highly enlarged acidic compartment.

Previous studies have shown that blocking endosomal maturation by knockdown of the early ESCRT component Hrs increases the size of immature endosomal class E compartments lacking ILVs and also results in increased BMP signaling (Piper et al., 1995; Jékely and Rørth, 2003; Chanut-Delalande et al., 2010). Our data demonstrate that elevated BMP signaling increases mMVBL size, suggesting that there is a complex bidirectional interaction between mMVBL maturation and size and the level of BMP signaling in SCs.

Our findings are consistent with a model in which BMP signaling also controls SC growth by driving endolysosomal trafficking and maturation events. Late endosomes and lysosomes have previously been shown to house major nutrient sensors and cell growth machinery, including the mTORC1 complex (Goberdhan, 2010; Ögmundsdóttir et al., 2012), which is activated by intraluminal amino acids. Interestingly, the growth rate of knockdown cells with reduced ESCRT function appears to correlate with mMVBL size (Fig. 5 I) rather than exosome secretion rate. We now need to test whether growth in these cells is mTORC1 dependent.

Whatever the explanation for the growth defects in SCs, our data very clearly implicate BMP signaling in the regulation of endolysosomal trafficking and exosome secretion. It will now be important to test whether BMP signaling plays a similar role in mammalian glands that secrete exosomes, such as prostate and breast, and determine whether this role is affected in diseases such as cancer.

Materials and methods

Fly stocks

The following stocks were used: *esgF/O^{ts}* (*esg-GAL4 tub-GAL80^{ts} UAS-FLP/CyO; UAS-GFP$_{nls}$ actin>FRT>CD2>FRT>GAL4/TM6* [Jiang et al., 2009]; a gift from B. Edgar, Center for Molecular Biology, University of Heidelberg, Heidelberg, Germany; *esg-GAL4^{NP7397}*, *tubP-GAL80^{ts}*, *P{UAS-FLP1.D}*, *P{UAS-GFP.nls}*, and *actin>FRT>CD2>FRT>GAL4/TM6* are described in FlyBase), *UAS–CD63-GFP* (Panáková et al., 2005; a C-terminal fusion of full-length human CD63 with pEGFP-C1, which was then inserted into the pUAST vector [Brand and Perrimon, 1993]; see FlyBase; a gift from S. Eaton, Max Planck Institute of Molecular Cell Biology and Genetics, Dresden, Germany), *tub-rab11-YFP*, *tub-rab7-YFP*, and *tub-rab5-YFP* (gifts from J.-P. Vincent, Medical Research Council National Institute for Medical Research, London, England, UK), *Acp26Aa-GAL4* (Chapman et al., 2003; ∼1.4-kb fragment upstream of the *Acp26Aa* coding region fused to GAL4; a gift from M. Wolfner, Cornell University, Ithaca, NY), *dsx-GAL4* (Rideout et al., 2010; a GAL4 gene trap inserted into the first coding exon of the *dsx* gene; a gift from S. Goodwin, University of Oxford, England, UK), *spi-GAL4* (Hayashi et al., 2002; *spi^{NP0261}*; see FlyBase), *UAS–ALiX-RNAi* (RNAi1, v32047 [Vienna Drosophila Resource Center]; RNAi2, HMS00298 [Bloomington Drosophila Stock Center] containing nonoverlapping target sequences; Dietzl et al., 2007; Ni et al., 2008), *UAS–Hrs-RNAi* (RNAi1, HMS00841 [Bloomington Drosophila Stock Center]; RNAi2, HMS00842 [Bloomington Drosophila Stock Center]; Ni et al., 2008), *UASp-YFP.Rab11.S25N* (Zhang et al., 2007; see FlyBase),

UASp-YFP.Rab7.T22N (Zhang et al., 2007; see FlyBase), *UAS–Rab35-RNAi* (JF02978), *UAS–Rab27-RNAi* (JF02165 [RNAi1] and HMS01523 [RNAi2] containing nonoverlapping target sequences), *UAS–Rab11-RNAi* (JF02812), *UAS–Rab7-RNAi* (JF02377), and *UAS–evi-RNAi* (RNAi1, 5214 [Vienna Drosophila Resource Center; Ni et al., 2008]; RNAi2 was a gift from J.-P. Vincent; Bloomington Drosophila Stock Center and Vienna Drosophila Resource Center RNAi lines are described in FlyBase), *protamineB-RFP-160* (Köttgen et al., 2011; full-length C-terminal fusion of *protamineB* and its upstream promoter to RFP; a gift from J. Belote, Syracuse University, Syracuse, NY), *tub-PI4KII-GFP* (Burgess et al., 2012; full-length *PI4KII* [LD24833] subcloned into a modified pCaSpeR4 vector containing the αTub84B promoter and with mEGFP inserted at its N-terminal end; a gift from J. Brill, The Hospital for Sick Children, Toronto, Ontario, Canada), *UAS-Dad* (Tsuneizumi et al., 1997; $Dad^{Scer\backslash UAS.cTa}$ in FlyBase), and *UAS-*Tkv^{QD} (Hoodless et al., 1996; full-length Thickveins coding sequence carrying a Q199D mutation cloned in the pUAST vector). *UAS–CD8-RFP*, *actin-GAL4*, and *tub-GAL80*^{ts} were obtained from the Bloomington Drosophila Stock Center. A *spi-GAL4* driver line (with or without *tub-GAL80*^{ts}), which expresses only in SCs within the AG, was used in all experiments except for exosome lumen counts (*dsx-GAL4 tub-GAL80*^{ts}; again specific for SCs in AG epithelium) and mating experiments, for which *esgF/O*^{ts} was used because it gives highly specific SC expression within the entire male reproductive system (Leiblich et al., 2012).

Classification of different vacuolar compartments in SCs

In living SCs, subcellular structures and intracompartment puncta are much better preserved than in fixed tissue (compare Fig. 1, E and G), so wherever possible, live staining was used for classifying and counting compartments. We expressed several UAS-regulated tagged markers for endolysosomal compartments in SCs, e.g., HRP-Lamp (Juhász et al., 2008) and spin-GFP (Sweeney and Davis, 2002), but they all altered the ratios of acidic and nonacidic compartments in these cells, so we could not use them as an additional tool to confirm our conclusion that large acidic compartments in SCs are late endosomes or lysosomes. CD63-GFP puncta that could be seen in the large acidic compartments of SCs were strongly fluorescent. This is consistent with observations in mammalian cells, in which CD63 is typically concentrated into ILVs within acidic MVBs before secretion (Escola et al., 1998).

Pulse–chase experiments

A short (8 h) pulse of CD63-GFP expression was induced by inhibiting the temperature-sensitive GAL4 transcriptional repressor GAL80^{ts} at 28.5°C. This was followed by a chase period at 18°C of 0–60 h. Note that the CD63-GFP transcript is likely to persist once the pulse has ended, and so, new fusion protein expression will continue during the chase period.

Analysis of exosome secretion and regulation

Because the AG lumen contains only nanoliter volumes of secreted fluid of complex composition (Fig. S2 G), including the exosomes made from just 40 SCs, it was not practical to use standard isolation approaches (Vlassov et al., 2012) to study SC exosomes. For in vivo exosome quantification and analysis of ANCE staining in the AG lumen (Figs. 5 and S4, respectively), newly eclosed males were incubated at 28.5°C to induce transgene expression. After 2 d, each male was mated to three w^{1118} virgin females overnight, after which the females were removed, and males were left for a further day before being dissected and fixed at 4 d after eclosion. This procedure allowed stored contents of the AG lumen to be partly expelled and replenished at least 2–3× during the period of transgene expression. Each test experiment was performed simultaneously with a control for direct comparison. The observation that blocking ESCRT-dependent events in SCs drastically reduces the levels of CD63-GFP in the AG lumen in young males after multiple matings without affecting expression in the gland (Fig. 5) strongly argues that shedding of membrane debris does not take place in these experiments. We used two RNAi's against Evi, a trafficking molecule required for secretion of Wingless on exosomes (Beckett et al., 2013), but not for CD63-positive exosome secretion (Gross et al., 2012), to test for nonspecific effects of modulating trafficking and RNAi overexpression. Although Evi is transcribed in many tissues in adults (Chintapalli et al., 2007), we have not confirmed that it is transcribed in SCs because an in situ hybridization method has not been developed for AG.

Mating experiments to analyze exosome transfer

For single-mating experiments to analyze exosome targets in the female reproductive tract (Figs. 6 and 7), w^{1118} or w^{1118}*; actin-GAL4; UAS–CD8-RFP* virgin females (2–10 d old) were placed with individual 3-d-old *spi-GAL4; UAS–CD63-GFP* ± *protamineB-RFP* virgin males, and matings were observed. Dissections of reproductive organs from females in 4% paraformaldehyde in PBS were performed at a known time after the start of mating. Dissected reproductive tracts were fixed for 30 min and then washed in PBST-0.03% (PBS and 0.03% Triton X-100) for 20 min before mounting in Vectashield with DAPI (Vector Laboratories). When dissected at 7 min after the start of mating, 2/8 female reproductive tracts did not contain CD63-GFP exosomes, suggesting that, despite sperm transfer from the testes, the contents of the AG had not yet been transferred to these individuals.

Sperm tails can also be marked in living flies with GFP-tagged proteins (Santel et al., 1997). However, although we constructed a UAS–CD63-mCherry transgenic line to study exosome fusion to sperm tails, we were unable to use this fly line successfully because the latter fusion protein aggregates in SCs and disrupts membrane trafficking.

Multiple-mating experiments

For analysis of the physiological role of exosomes in reproduction (Fig. 8), multiple-mating experiments were performed as previously reported (Leiblich et al., 2012); this protocol is described in this paragraph. Control and test experiments were always performed simultaneously to account for variations in food and other conditions. Newly eclosed virgin males (*esgF/O*^{ts}*>ALiX-RNAi 1*, *esgF/O*^{ts}*>Rab11DN*, or *esgF/O*^{ts}) were shifted to 28.5°C to induce transgene expression. Individual males were then added after 3 d to five 2–10-d-old virgin w^{1118} females (for a specific group of control and test flies, females were of identical age) overnight at 28.5°C. The next morning, these females were then replaced with three 2–5-d-old virgin w^{1118} females for 3 h and watched to score timing of mating events, after which the females were separated and incubated at 25°C. For crosses in which at least two females had mated, these females were transferred to separate, fresh vials on each of the next 3 d. Egg counts and progeny counts were recorded for each vial. Each female was then introduced to a dominantly marked (*CyO Roi*) white-eyed male and left for 3 h. Remating events were confirmed by the presence of *CyO Roi* progeny. The absence of effects on egg laying and fertility in males in which exosome secretion is inhibited supports the conclusion that the secretion of most seminal proteins is unaffected by this treatment.

LysoTracker staining

Glands were dissected in ice-cold PBS and left in ice-cold 5 µM LysoTracker red DND-99 (Invitrogen) in PBS for 5 min. They were then washed in ice-cold PBS for 5 min and mounted in PBS using a coverslip bridge for imaging. These specimens were imaged within 1 h but showed no signs of cell death or deterioration over several hours.

Preparation of AGs for antibody staining

The age of dissected flies is given as days after eclosion at 28.5°C. Immunostaining of the AG was performed as previously reported (Leiblich et al., 2012). Dissections were performed in 4% paraformaldehyde in PBS with a minimum total fixation period of 15 min followed by a 20-min wash in PBST-0.3% and then a 30-min wash in PBSTG-male (PBST-0.3% and 10% goat serum). All washes were performed at room temperature (22°C).

Preparation of female reproductive tract for staining

Females were dissected at a fixed time after the start of mating in ice-cold PBS and then fixed in 4% paraformaldehyde in PBS at 22°C. Tracts were washed for 6 × 5 min in PBST-0.3% before incubation in 100 µl chitinase solution (*Streptomyces griseus*; Sigma-Aldrich; 6 U/ml in PBST-0.3%) for 2 h at 22°C (Lung and Wolfner, 1999). Tracts were washed in PBST-0.3% for 6 × 5 min and then refixed for 20 min at 22°C. They were washed again in PBST-0.3% (3 × 5 min) and then blocked for 2 h with gentle shaking at room temperature in 100 µl PBSTG-female (PBS, 0.5% Triton X-100, 3% goat serum, and 0.1% BSA). All washes were performed at room temperature (22°C).

Immunostaining

Samples were incubated with primary antibodies (diluted in the appropriate PBST) overnight at 4°C before washing in appropriate PBST (6 × 10 min). They were then incubated for 2 h at 22°C with fluorescently conjugated donkey secondary antibodies (1:400 dilution; Alexa Fluor 649 and Cy3 labeled; Jackson ImmunoResearch Laboratories, Inc.) before six further 10-min washes in PBST. Stained glands were mounted in Vectashield with DAPI. The following primary antibodies were used: mouse anti–discs large (1:10 dilution of supernatant; Developmental Studies Hybridoma Bank), mouse anti-CD63 (1:10; Developmental Studies Hybridoma Bank), rabbit anti-GFP (1:1,000; catalog no. 6556; Abcam), mouse anti-Fas3

(1:10; Developmental Studies Hybridoma Bank; Narasimha et al., 2008), polyclonal rabbit anti-Rab7 (1:3,000; Tanaka and Nakamura, 2008; a gift from A. Nakamura, RIKEN Center for Developmental Biology, Kobe, Japan), and rat anti-ANCE (1:2,000; Rylett et al., 2007; a gift from E. Isaac, University of Leeds, Leeds, England, UK). All washes were performed at room temperature (22°C). Fluorescent GFP puncta were more readily observed in the female reproductive tract, perhaps because the luminal microenvironment (e.g., pH) affects fluorescence levels.

Western blot analysis

Protein extraction. For male AG samples, 3-d-old virgin *dsx-GAL4; tubGAL80^{ts}; UAS–CD63-GFP* males (incubated at 29°C from eclosion) expressing *UAS–ALiX-RNAi*, *UAS–Hrs-RNAi*, or *UAS-Rab11DN* constructs were dissected in ice-cold PBS. *w^{1118}* virgin males were used as a negative control.

For female samples, these males were introduced to single *w^{1118}* virgin females, and matings were observed. The whole female reproductive tracts with the ovaries removed were dissected in ice-cold PBS immediately after the end of mating. *w^{1118}* virgin females and *w^{1118}* females mated to *w^{1118}* males were used as a negative controls.

AG proteins were extracted by homogenizing the glands using a polycarbonate pestle on ice in 100 µl lysis buffer (radioimmunoprecipitation assay buffer; Sigma-Aldrich) supplemented with antiprotease and antiphosphatase cocktails (Sigma-Aldrich). The crude lysates were centrifuged briefly (300 *g*; 5 min), and the protein-containing supernatant was extracted. Proteins were quantified using a bicinchoninic acid assay kit (Thermo Fisher Scientific).

Blotting. Blotting of AG proteins was performed as previously described (Rylett et al., 2007), with minor alterations; the protocol is described in this paragraph. Samples containing 2.5 µg homogenized protein (made up to 15 µl) were added to 5 µl of 4× sampling buffer (0.2 M Tris-HCl, pH 6.8, 12% SDS, 40% glycerol, 20% β-mercaptoethanol, and 0.008% bromophenol blue) and heated to 95°C for 5 min. Proteins were separated using 10% mini-Protean TGX precast gels (Bio-Rad Laboratories) for 30 min along with a prestained ladder (Precision Plus Protein Dual Color Standards). Separated proteins were transferred to a polyvinylidene fluoride membrane (Immobilon-P; EMD Millipore) at 100 V for 1 h. The polyvinylidene fluoride membrane was then blocked for 1 h in 5% skimmed milk in TBS with Tween 20 (TBST) and then incubated with the anti-ANCE antibody (Rylett at al. 2007) at a 1:1,000 dilution, anti-GFP at 1:500 (rabbit; ab6556; Abcam), or anti-actin 1:10,000 (rabbit; 04-1040; EMD Millipore) in 5% milk in TBST overnight at 4°C. The membrane was washed in TBST for 3 × 5 min, incubated at room temperature for 1 h with a HRP-conjugated anti–rabbit secondary antibody (W4018; Promega) at 1:20,000 in 5% milk in TBST, and then washed in TBST for 3 × 5 min. Bound anti-ANCE, anti-GFP, or anti-actin antibody was detected using a SuperSignal West Pico Chemiluminescent Substrate kit (Thermo Fisher Scientific) as described in the manufacturer's instructions. Photographic films were exposed to the membrane for 30 s to 1 min before film development. Band intensities were calculated using ImageJ (National Institutes of Health).

Imaging

Live and fixed samples were imaged on a scanning confocal microscope (LSM 510 Meta [Axioplan 2]; Carl Zeiss), using LSM 510 Meta software. Low magnification images (Figs. 1, A and B; 6 D; and 7 B) were obtained using the 10× dry objective (0.45 NA Plan Apochromat); all other confocal images were obtained using the 63× objective (1.4 NA oil differential interference contrast Plan Apochromat) with immersion oil (Carl Zeiss). All live imaging was performed at 16°C. Fixed imaging was performed at 21°C. Details of fluorochromes used in individual experiments are described in the immunostaining procedure and figure legends.

Largest mMVBL diameter was measured on ImageJ by selecting the widest diameter of the largest compartment in a confocal z series. Quantifications of secreted CD63-GFP puncta (Figs. 5 A and S4 A) were performed using ImageJ particle analysis. Fluorescence intensity analysis of lumen content (Fig. S4 G) was performed using Photoshop (Adobe) software (gray intensity mean). Time series Videos 1 and 2 were recorded using LSM Image Browser after cropping video frames. Maximal projection image processing was performed on ImageJ, and rotating 3D projections shown in Videos 3 and 4 were recorded using the ImageJ 3D Viewer to process confocal z series image files. All other confocal images were processed using LSM Image Browser.

For exosome lumen counts and ANCE staining intensity quantification, three stacked confocal images of the lumen were obtained at 5-µm intervals within the central third of each gland at a 1.7× zoom, using the 63× objective. Glands were imaged at gain settings to minimize background staining and, for exosome counts, were repeated at a lower gain setting (Fig. S4 A) to confirm that decreased numbers of puncta did not represent a reduced number of more intensely fluorescent structures. *Rab11DN* is not secreted into the AG lumen (Fig. S5, B versus A), so the limited number of fluorescent puncta in the lumen in this genetic background represents CD63-GFP–positive structures. The values represent the mean particles in a 7,225-µm^2 luminal area, averaged over a minimum of nine glands, and calculated as a percentage of the control value from a parallel experiment.

For nuclear size data, 10 glands for each genotype were analyzed. For each gland, the areas of nuclei for three different SCs, and for each SC, nuclear areas for three surrounding MCs, were measured using ImageJ by outlining nuclei and measuring the enclosed area. For each SC, the mean nuclear size of neighboring MCs was calculated, and relative nuclear size values were obtained by dividing each SC value by the corresponding MC value. These ratios were averaged across 10 glands to give the mean nuclear size ratio. Individual experimental genotypes were always analyzed in parallel with a control that did not express the transgene.

EM

3-d-old *w^{1118}* male reproductive tracts were dissected out and stored overnight in fixative containing 2.5% glutaraldehyde and 4% formaldehyde in PBS, pH 7.2, washed with PBS, postfixed with 1% osmium tetroxide, dehydrated, and embedded in Spurr's epoxy resin between two sheets of polythene. Ultrathin sections were prepared with an ultratome (Ultracut S; Reichert), mounted on formvar-coated slot grids, stained with 2% uranyl acetate and lead citrate, and examined with an electron microscope (1010; JEOL) operated at 80 kV. Although several methodologies for fixation were tested, membranes in AG preparations were often poorly preserved.

Statistical analysis

All compartment and exosome counts, as well as nuclear and mMVBL size measurements, involved analysis of SCs from multiple independent animals and were repeated in at least three separate experiments. Data were analyzed using Excel (Microsoft) or SPSS (IBM). Normality of the data was assessed using a Shapiro–Wilk test. Based on this test, data were analyzed using a two-tailed unpaired Student's *t* test or Mann–Whitney *U* test for single-pair comparisons. Remating data and mating times (Fig. 8) were analyzed using Fisher's exact test. Remating results shown are from a single representative experiment including pooled data collected from crosses set up over several days. These experiments were repeated twice.

Online supplemental material

Fig. S1 shows SC-specific secretion of CD63-GFP exosomes and characterization of SC vacuolar compartments. Fig. S2 shows colocalization of GFP with the anti-CD63 antibody signal, except in specific mMVBLs. Fig. S3 shows individual channels from a pulse–chase analysis in Fig. 3 (A–F). Fig. S4 shows the effects of knocking down membrane trafficking regulators on ANCE secretion. Fig. S5 shows transfer of SC-specific CD63-GFP to neighboring MCs and the absence of Rab11-YFP on exosomes. Video 1 depicts a live-imaging sequence showing an acidic mMVBL fusing to a nonacidic SV in SCs (Fig. 4 A). Video 2 depicts a live-imaging sequence showing invagination of a CD63-GFP–positive membrane from the mMVBL limiting membrane (Fig. 4 B). Video 3 shows a rotating 3D projection of the image shown in Fig. 6 G. Video 4 shows a rotating 3D projection of the image in Fig. 7 C. Online supplemental material is available at http://www.jcb.org/cgi/content/full/jcb.201401072/DC1. Additional data are available in the JCB DataViewer at http://dx.doi.org/10.1083/jcb.201401072.dv.

We thank Stephen Goodwin, Suzanne Eaton, Mariana Wolfner, Jean-Paul Vincent, Elwyn Isaac, Bruce Edgar, Akira Nakamura, Julie Brill, and John Belote for stocks and reagents; Bloomington Drosophila Stock Center, Vienna Drosophila Resource Center, and Drosophila Genomics Resource Center stock centers for flies; Developmental Studies Hybridoma Bank, Iowa for monoclonal antibodies; Ana-Maria Vallés, Richard Parton, and the Micron Oxford Bioimaging facility for assistance with live imaging; and Yael Heifitz for advice regarding female reproductive tract staining.

This work was supported by the Wellcome Trust (092927/Z/10/Z and a studentship to L. Corrigan), the Oxford Cancer Research Centre (OCRC; Cancer Research UK clinical training fund), Cancer Research UK (C38302/A12278) through the OCRC Development Fund, the Biotechnology and Biological Sciences Research Council (BB/K017462/1), a Medical Research Council studentship to S. Redhai, and a studentship to S.M.W. Perera from The British Province of the Society of Jesus (626791).

The authors declare no competing financial interests.

Submitted: 17 January 2014
Accepted: 31 July 2014

References

Aalberts, M., E. Sostaric, R. Wubbolts, M.W.M. Wauben, E.N.M. Nolte-'t Hoen, B.M. Gadella, T.A.E. Stout, and W. Stoorvogel. 2013. Spermatozoa recruit prostasomes in response to capacitation induction. *Biochim. Biophys. Acta*. 1834:2326–2335. http://dx.doi.org/10.1016/j.bbapap.2012.08.008

Arienti, G., E. Carlini, and C.A. Palmerini. 1997. Fusion of human sperm to prostasomes at acidic pH. *J. Membr. Biol.* 155:89–94. http://dx.doi.org/10.1007/s002329900160

Avila, F.W., K. Ravi Ram, M.C. Bloch Qazi, and M.F. Wolfner. 2010. Sex peptide is required for the efficient release of stored sperm in mated *Drosophila* females. *Genetics*. 186:595–600. http://dx.doi.org/10.1534/genetics.110.119735

Azmi, A.S., B. Bao, and F.H. Sarkar. 2013. Exosomes in cancer development, metastasis, and drug resistance: a comprehensive review. *Cancer Metastasis Rev.* 32:623–642. http://dx.doi.org/10.1007/s10555-013-9441-9

Baietti, M.F., Z. Zhang, E. Mortier, A. Melchior, G. Degeest, A. Geeraerts, Y. Ivarsson, F. Depoortere, C. Coomans, E. Vermeiren, et al. 2012. Syndecan-syntenin-ALIX regulates the biogenesis of exosomes. *Nat. Cell Biol.* 14:677–685. http://dx.doi.org/10.1038/ncb2502

Beckett, K., S. Monier, L. Palmer, C. Alexandre, H. Green, E. Bonneil, G. Raposo, P. Thibault, R. Le Borgne, and J.-P. Vincent. 2013. *Drosophila* S2 cells secrete wingless on exosome-like vesicles but the wingless gradient forms independently of exosomes. *Traffic*. 14:82–96.

Bertram, M.J., G.A. Akerkar, R.L. Ard, C. Gonzalez, and M.F. Wolfner. 1992. Cell type-specific gene expression in the *Drosophila melanogaster* male accessory gland. *Mech. Dev.* 38:33–40. http://dx.doi.org/10.1016/0925-4773(92)90036-J

Brand, A.H., and N. Perrimon. 1993. Targeted gene expression as a means of altering cell fates and generating dominant phenotypes. *Development*. 118:401–415.

Burgess, J., L.M. Del Bel, C.-I.J. Ma, B. Barylko, G. Polevoy, J. Rollins, J.P. Albanesi, H. Krämer, and J.A. Brill. 2012. Type II phosphatidylinositol 4-kinase regulates trafficking of secretory granule proteins in *Drosophila*. *Development*. 139:3040–3050. http://dx.doi.org/10.1242/dev.077644

Chanut-Delalande, H., A.C. Jung, M.M. Baer, L. Lin, F. Payre, and M. Affolter. 2010. The Hrs/Stam complex acts as a positive and negative regulator of RTK signaling during *Drosophila* development. *PLoS ONE*. 5:e10245. http://dx.doi.org/10.1371/journal.pone.0010245

Chapman, T., J. Bangham, G. Vinti, B. Seifried, O. Lung, M.F. Wolfner, H.K. Smith, and L. Partridge. 2003. The sex peptide of *Drosophila melanogaster*: female post-mating responses analyzed by using RNA interference. *Proc. Natl. Acad. Sci. USA*. 100:9923–9928. http://dx.doi.org/10.1073/pnas.1631635100

Chen, P.S., E. Stumm-Zollinger, T. Aigaki, J. Balmer, M. Bienz, and P. Böhlen. 1988. A male accessory gland peptide that regulates reproductive behavior of female *D. melanogaster*. *Cell*. 54:291–298. http://dx.doi.org/10.1016/0092-8674(88)90192-4

Chen, W., Y. Feng, D. Chen, and A. Wandinger-Ness. 1998. Rab11 is required for trans-golgi network-to-plasma membrane transport and a preferential target for GDP dissociation inhibitor. *Mol. Biol. Cell*. 9:3241–3257. http://dx.doi.org/10.1091/mbc.9.11.3241

Chintapalli, V.R., J. Wang, and J.A.T. Dow. 2007. Using FlyAtlas to identify better *Drosophila melanogaster* models of human disease. *Nat. Genet.* 39:715–720. http://dx.doi.org/10.1038/ng2049

Christianson, H.C., K.J. Svensson, and M. Belting. 2014. Exosome and microvesicle mediated phene transfer in mammalian cells. *Semin. Cancer Biol.* http://dx.doi.org/10.1016/j.semcancer.2014.04.007

Colombo, M., C. Moita, G. van Niel, J. Kowal, J. Vigneron, P. Benaroch, N. Manel, L.F. Moita, C. Théry, and G. Raposo. 2013. Analysis of ESCRT functions in exosome biogenesis, composition and secretion highlights the heterogeneity of extracellular vesicles. *J. Cell Sci.* 126:5553–5565. http://dx.doi.org/10.1242/jcs.128868

DiBenedetto, A.J., H.A. Harada, and M.F. Wolfner. 1990. Structure, cell-specific expression, and mating-induced regulation of a *Drosophila melanogaster* male accessory gland gene. *Dev. Biol.* 139:134–148. http://dx.doi.org/10.1016/0012-1606(90)90284-P

Dietzl, G., D. Chen, F. Schnorrer, K.-C. Su, Y. Barinova, M. Fellner, B. Gasser, K. Kinsey, S. Oppel, S. Scheiblauer, et al. 2007. A genome-wide transgenic RNAi library for conditional gene inactivation in *Drosophila*. *Nature*. 448:151–156. http://dx.doi.org/10.1038/nature05954

Dores, M.R., M.M. Paing, H. Lin, W.A. Montagne, A. Marchese, and J. Trejo. 2012. AP-3 regulates PAR1 ubiquitin-independent MVB/lysosomal sorting via an ALIX-mediated pathway. *Mol. Biol. Cell*. 23:3612–3623. http://dx.doi.org/10.1091/mbc.E12-03-0251

Edgar, J.R., E.R. Eden, and C.E. Futter. 2014. Hrs- and CD63-dependent competing mechanisms make different sized endosomal intraluminal vesicles. *Traffic*. 15:197–211. http://dx.doi.org/10.1111/tra.12139

Escola, J.M., M.J. Kleijmeer, W. Stoorvogel, J.M. Griffith, O. Yoshie, and H.J. Geuze. 1998. Selective enrichment of tetraspan proteins on the internal vesicles of multivesicular endosomes and on exosomes secreted by human B-lymphocytes. *J. Biol. Chem.* 273:20121–20127. http://dx.doi.org/10.1074/jbc.273.32.20121

Fabiani, R., L. Johansson, O. Lundkvist, and G. Ronquist. 1994. Enhanced recruitment of motile spermatozoa by prostasome inclusion in swim-up medium. *Hum. Reprod.* 9:1485–1489.

Fader, C.M., A. Savina, D. Sánchez, and M.I. Colombo. 2005. Exosome secretion and red cell maturation: Exploring molecular components involved in the docking and fusion of multivesicular bodies in K562 cells. *Blood Cells Mol. Dis.* 35:153–157. http://dx.doi.org/10.1016/j.bcmd.2005.07.002

Ge, R., E. Tan, S. Sharghi-Namini, and H.H. Asada. 2012. Exosomes in cancer microenvironment and beyond: Have we overlooked these extracellular messengers? *Cancer Microenviron*. 5:323–332. http://dx.doi.org/10.1007/s12307-012-0110-2

Gligorov, D., J.L. Sitnik, R.K. Maeda, M.F. Wolfner, and F. Karch. 2013. A novel function for the Hox gene *Abd-B* in the male accessory gland regulates the long-term female post-mating response in *Drosophila*. *PLoS Genet.* 9:e1003395. http://dx.doi.org/10.1371/journal.pgen.1003395

Goberdhan, D.C. 2010. Intracellular amino acid sensing and mTORC1-regulated growth: new ways to block an old target? *Curr. Opin. Investig. Drugs*. 11:1360–1367.

Gross, J.C., V. Chaudhary, K. Bartscherer, and M. Boutros. 2012. Active Wnt proteins are secreted on exosomes. *Nat. Cell Biol.* 14:1036–1045. http://dx.doi.org/10.1038/ncb2574

Hayashi, S., K. Ito, Y. Sado, M. Taniguchi, A. Akimoto, H. Takeuchi, T. Aigaki, F. Matsuzaki, H. Nakagoshi, T. Tanimura, et al. 2002. GETDB, a database compiling expression patterns and molecular locations of a collection of Gal4 enhancer traps. *Genesis*. 34:58–61. http://dx.doi.org/10.1002/gene.10137

Hirota, Y., T. Kuronita, H. Fujita, and Y. Tanaka. 2007. A role for Rab5 activity in the biogenesis of endosomal and lysosomal compartments. *Biochem. Biophys. Res. Commun.* 364:40–47. http://dx.doi.org/10.1016/j.bbrc.2007.09.089

Hoodless, P.A., T. Haerry, S. Abdollah, M. Stapleton, M.B. O'Connor, L. Attisano, and J.L. Wrana. 1996. MADR1, a MAD-related protein that functions in BMP2 signaling pathways. *Cell*. 85:489–500. http://dx.doi.org/10.1016/S0092-8674(00)81250-7

Hsu, C., Y. Morohashi, S. Yoshimura, N. Manrique-Hoyos, S. Jung, M.A. Lauterbach, M. Bakhti, M. Grønborg, W. Möbius, J. Rhee, et al. 2010. Regulation of exosome secretion by Rab35 and its GTPase-activating proteins TBC1D10A–C. *J. Cell Biol.* 189:223–232. http://dx.doi.org/10.1083/jcb.200911018

Jékely, G., and P. Rørth. 2003. Hrs mediates downregulation of multiple signalling receptors in *Drosophila*. *EMBO Rep.* 4:1163–1168. http://dx.doi.org/10.1038/sj.embor.7400019

Jiang, H., P.H. Patel, A. Kohlmaier, M.O. Grenley, D.G. McEwen, and B.A. Edgar. 2009. Cytokine/Jak/Stat signaling mediates regeneration and homeostasis in the *Drosophila* midgut. *Cell*. 137:1343–1355. http://dx.doi.org/10.1016/j.cell.2009.05.014

Juhász, G., J.H. Hill, Y. Yan, M. Sass, E.H. Baehrecke, J.M. Backer, and T.P. Neufeld. 2008. The class III PI(3)K Vps34 promotes autophagy and endocytosis but not TOR signaling in *Drosophila*. *J. Cell Biol.* 181:655–666. http://dx.doi.org/10.1083/jcb.200712051

Katzmann, D.J., C.J. Stefan, M. Babst, and S.D. Emr. 2003. Vps27 recruits ESCRT machinery to endosomes during MVB sorting. *J. Cell Biol.* 162:413–423. http://dx.doi.org/10.1083/jcb.200302136

Kershaw-Young, C.M., X. Druart, J. Vaughan, and W.M.C. Maxwell. 2012. β-Nerve growth factor is a major component of alpaca seminal plasma and induces ovulation in female alpacas. *Reprod. Fertil. Dev.* 24:1093–1097. http://dx.doi.org/10.1071/RD12039

Koles, K., J. Nunnari, C. Korkut, R. Barria, C. Brewer, Y. Li, J. Leszyk, B. Zhang, and V. Budnik. 2012. Mechanism of evenness interrupted (Evi)-exosome release at synaptic boutons. *J. Biol. Chem.* 287:16820–16834. http://dx.doi.org/10.1074/jbc.M112.342667

Köttgen, M., A. Hofherr, W. Li, K. Chu, S. Cook, C. Montell, and T. Watnick. 2011. *Drosophila* sperm swim backwards in the female reproductive tract and are activated via TRPP2 ion channels. *PLoS ONE*. 6:e20031. http://dx.doi.org/10.1371/journal.pone.0020031

Kubli, E. 2003. Sex-peptides: seminal peptides of the *Drosophila* male. *Cell. Mol. Life Sci.* 60:1689–1704. http://dx.doi.org/10.1007/s00018-003-3052

Lance, R.S., R.R. Drake, and D.A. Troyer. 2011. Multiple recognition assay reveals prostasomes as promising plasma biomarkers for prostate cancer. *Expert Rev. Anticancer Ther.* 11:1341–1343. http://dx.doi.org/10.1586/era.11.134

Leiblich, A., L. Marsden, C. Gandy, L. Corrigan, R. Jenkins, F. Hamdy, and C. Wilson. 2012. Bone morphogenetic protein- and mating-dependent

secretory cell growth and migration in the *Drosophila* accessory gland. *Proc. Natl. Acad. Sci. USA*. 109:19292–19297. http://dx.doi.org/10.1073/pnas.1214517109

Liu, H., and E. Kubli. 2003. Sex-peptide is the molecular basis of the sperm effect in *Drosophila melanogaster*. *Proc. Natl. Acad. Sci. USA*. 100:9929–9933. http://dx.doi.org/10.1073/pnas.1631700100

Lloyd, T.E., R. Atkinson, M.N. Wu, Y. Zhou, G. Pennetta, and H.J. Bellen. 2002. Hrs regulates endosome membrane invagination and tyrosine kinase receptor signaling in *Drosophila*. *Cell*. 108:261–269. http://dx.doi.org/10.1016/S0092-8674(02)00611-6

Lung, O., and M.F. Wolfner. 1999. *Drosophila* seminal fluid proteins enter the circulatory system of the mated female fly by crossing the posterior vaginal wall. *Insect Biochem. Mol. Biol.* 29:1043–1052. http://dx.doi.org/10.1016/S0965-1748(99)00078-8

Marois, E., A. Mahmoud, and S. Eaton. 2006. The endocytic pathway and formation of the Wingless morphogen gradient. *Development*. 133:307–317. http://dx.doi.org/10.1242/dev.02197

Matsuo, H., J. Chevallier, N. Mayran, I. Le Blanc, C. Ferguson, J. Fauré, N.S. Blanc, S. Matile, J. Dubochet, R. Sadoul, et al. 2004. Role of LBPA and Alix in multivesicular liposome formation and endosome organization. *Science*. 303:531–534. http://dx.doi.org/10.1126/science.1092425

Minami, R., M. Wakabayashi, S. Sugimori, K. Taniguchi, A. Kokuryo, T. Imano, T. Adachi-Yamada, N. Watanabe, and H. Nakagoshi. 2012. The homeodomain protein defective proventriculus is essential for male accessory gland development to enhance fecundity in *Drosophila*. *PLoS ONE*. 7:e32302. http://dx.doi.org/10.1371/journal.pone.0032302

Minogue, S., M.G. Waugh, M.A. De Matteis, D.J. Stephens, F. Berditchevski, and J.J. Hsuan. 2006. Phosphatidylinositol 4-kinase is required for endosomal trafficking and degradation of the EGF receptor. *J. Cell Sci.* 119:571–581. http://dx.doi.org/10.1242/jcs.02752

Morelli, A.E., A.T. Larregina, W.J. Shufesky, M.L.G. Sullivan, D.B. Stolz, G.D. Papworth, A.F. Zahorchak, A.J. Logar, Z. Wang, S.C. Watkins, et al. 2004. Endocytosis, intracellular sorting, and processing of exosomes by dendritic cells. *Blood*. 104:3257–3266. http://dx.doi.org/10.1182/blood-2004-03-0824

Narasimha, M., A. Uv, A. Krejci, N.H. Brown, and S.J. Bray. 2008. Grainy head promotes expression of septate junction proteins and influences epithelial morphogenesis. *J. Cell Sci.* 121:747–752. http://dx.doi.org/10.1242/jcs.019422

Ni, J.-Q., M. Markstein, R. Binari, B. Pfeiffer, L.-P. Liu, C. Villalta, M. Booker, L. Perkins, and N. Perrimon. 2008. Vector and parameters for targeted transgenic RNA interference in *Drosophila melanogaster*. *Nat. Methods*. 5:49–51. http://dx.doi.org/10.1038/nmeth1146

Nilsson, J., J. Skog, A. Nordstrand, V. Baranov, L. Mincheva-Nilsson, X.O. Breakefield, and A. Widmark. 2009. Prostate cancer-derived urine exosomes: a novel approach to biomarkers for prostate cancer. *Br. J. Cancer*. 100:1603–1607. http://dx.doi.org/10.1038/sj.bjc.6605058

Odorizzi, G. 2006. The multiple personalities of Alix. *J. Cell Sci.* 119:3025–3032. http://dx.doi.org/10.1242/jcs.03072

Ögmundsdóttir, M.H., S. Heublein, S. Kazi, B. Reynolds, S.M. Visvalingam, M.K. Shaw, and D.C.I. Goberdhan. 2012. Proton-assisted amino acid transporter PAT1 complexes with Rag GTPases and activates TORC1 on late endosomal and lysosomal membranes. *PLoS ONE*. 7:e36616. http://dx.doi.org/10.1371/journal.pone.0036616

Ostrowski, M., N.B. Carmo, S. Krumeich, I. Fanget, G. Raposo, A. Savina, C.F. Moita, K. Schauer, A.N. Hume, R.P. Freitas, et al. 2010. Rab27a and Rab27b control different steps of the exosome secretion pathway. *Nat. Cell Biol.* 12:19–30. http://dx.doi.org/10.1038/ncb2000

Palmerini, C.A., E. Carlini, A. Nicolucci, and G. Arienti. 1999. Increase of human spermatozoa intracellular Ca2+ concentration after fusion with prostasomes. *Cell Calcium*. 25:291–296. http://dx.doi.org/10.1054/ceca.1999.0031

Panáková, D., H. Sprong, E. Marois, C. Thiele, and S. Eaton. 2005. Lipoprotein particles are required for Hedgehog and Wingless signalling. *Nature*. 435:58–65. http://dx.doi.org/10.1038/nature03504

Park, K.-H., B.-J. Kim, J. Kang, T.-S. Nam, J.M. Lim, H.T. Kim, J.K. Park, Y.G. Kim, S.-W. Chae, and U.-H. Kim. 2011. Ca2+ signaling tools acquired from prostasomes are required for progesterone-induced sperm motility. *Sci. Signal*. 4:ra31. http://dx.doi.org/10.1126/scisignal.2001595

Peng, J., S. Chen, S. Büsser, H. Liu, T. Honegger, and E. Kubli. 2005. Gradual release of sperm bound sex-peptide controls female postmating behavior in *Drosophila*. *Curr. Biol.* 15:207–213. http://dx.doi.org/10.1016/j.cub.2005.01.034

Piper, R.C., A.A. Cooper, H. Yang, and T.H. Stevens. 1995. VPS27 controls vacuolar and endocytic traffic through a prevacuolar compartment in *Saccharomyces cerevisiae*. *J. Cell Biol.* 131:603–617. http://dx.doi.org/10.1083/jcb.131.3.603

Properzi, F., M. Logozzi, and S. Fais. 2013. Exosomes: the future of biomarkers in medicine. *Biomarkers Med.* 7:769–778. http://dx.doi.org/10.2217/bmm.13.63

Raposo, G., and W. Stoorvogel. 2013. Extracellular vesicles: Exosomes, microvesicles, and friends. *J. Cell Biol.* 200:373–383. http://dx.doi.org/10.1083/jcb.201211138

Ravi Ram, K., S. Ji, and M.F. Wolfner. 2005. Fates and targets of male accessory gland proteins in mated female *Drosophila melanogaster*. *Insect Biochem. Mol. Biol.* 35:1059–1071. http://dx.doi.org/10.1016/j.ibmb.2005.05.001

Record, M., K. Carayon, M. Poirot, and S. Silvente-Poirot. 2014. Exosomes as new vesicular lipid transporters involved in cell-cell communication and various pathophysiologies. *Biochim. Biophys. Acta*. 1841:108–120. http://dx.doi.org/10.1016/j.bbalip.2013.10.004

Rideout, E.J., A.J. Dornan, M.C. Neville, S. Eadie, and S.F. Goodwin. 2010. Control of sexual differentiation and behavior by the doublesex gene in *Drosophila melanogaster*. *Nat. Neurosci.* 13:458–466. http://dx.doi.org/10.1038/nn.2515

Rodríguez-Martínez, H., U. Kvist, J. Ernerudh, L. Sanz, and J.J. Calvete. 2011. Seminal plasma proteins: what role do they play? *Am. J. Reprod. Immunol.* 66(Suppl. 1):11–22. http://dx.doi.org/10.1111/j.1600-0897.2011.01033.x

Ronquist, G. 2012. Prostasomes are mediators of intercellular communication: from basic research to clinical implications. *J. Intern. Med.* 271:400–413. http://dx.doi.org/10.1111/j.1365-2796.2011.02487.x

Ronquist, K.G., G. Ronquist, A. Larsson, and L. Carlsson. 2010. Proteomic analysis of prostate cancer metastasis-derived prostasomes. *Anticancer Res.* 30:285–290.

Rylett, C.M., M.J. Walker, G.J. Howell, A.D. Shirras, and R.E. Isaac. 2007. Male accessory glands of *Drosophila melanogaster* make a secreted angiotensin I-converting enzyme (ANCE), suggesting a role for the peptide-processing enzyme in seminal fluid. *J. Exp. Biol.* 210:3601–3606. http://dx.doi.org/10.1242/jeb.009035

Sahlén, G., A. Ahlander, A. Frost, G. Ronquist, B.J. Norlén, and B.O. Nilsson. 2004. Prostasomes are secreted from poorly differentiated cells of prostate cancer metastases. *Prostate*. 61:291–297. http://dx.doi.org/10.1002/pros.20090

Santel, A., T. Winhauer, N. Blümer, and R. Renkawitz-Pohl. 1997. The *Drosophila* don juan (dj) gene encodes a novel sperm specific protein component characterized by an unusual domain of a repetitive amino acid motif. *Mech. Dev.* 64:19–30. http://dx.doi.org/10.1016/S0925-4773(97)00031-2

Savina, A., M. Vidal, and M.I. Colombo. 2002. The exosome pathway in K562 cells is regulated by Rab11. *J. Cell Sci.* 115:2505–2515.

Savina, A., C.M. Fader, M.T. Damiani, and M.I. Colombo. 2005. Rab11 promotes docking and fusion of multivesicular bodies in a calcium-dependent manner. *Traffic*. 6:131–143. http://dx.doi.org/10.1111/j.1600-0854.2004.00257.x

Schroeder, B., S. Srivatsan, A. Shaw, D. Billadeau, and M.A. McNiven. 2012. CIN85 phosphorylation is essential for EGFR ubiquitination and sorting into multivesicular bodies. *Mol. Biol. Cell*. 23:3602–3611. http://dx.doi.org/10.1091/mbc.E11-08-0666

Sirot, L.K., M.C. Hardstone, M.E.H. Helinski, J.M.C. Ribeiro, M. Kimura, P. Deewatthanawong, M.F. Wolfner, and L.C. Harrington. 2011. Towards a semen proteome of the dengue vector mosquito: protein identification and potential functions. *PLoS Negl. Trop. Dis.* 5:e989. http://dx.doi.org/10.1371/journal.pntd.0000989

Soekmadji, C., P.J. Russell, and C.C. Nelson. 2013. Exosomes in prostate cancer: putting together the pieces of a puzzle. *Cancers (Basel)*. 5:1522–1544. http://dx.doi.org/10.3390/cancers5041522

Stenmark, H. 2009. Rab GTPases as coordinators of vesicle traffic. *Nat. Rev. Mol. Cell Biol.* 10:513–525. http://dx.doi.org/10.1038/nrm2728

Stenmark, H., R.G. Parton, O. Steele-Mortimer, A. Lütcke, J. Gruenberg, and M. Zerial. 1994. Inhibition of rab5 GTPase activity stimulates membrane fusion in endocytosis. *EMBO J.* 13:1287–1296.

Sullivan, R., and F. Saez. 2013. Epididymosomes, prostasomes, and liposomes: their roles in mammalian male reproductive physiology. *Reproduction*. 146:R21–R35. http://dx.doi.org/10.1530/REP-13-0058

Sweeney, S.T., and G.W. Davis. 2002. Unrestricted synaptic growth in spinster-a late endosomal protein implicated in TGF-beta-mediated synaptic growth regulation. *Neuron*. 36:403–416. http://dx.doi.org/10.1016/S0896-6273(02)01014-0

Tamai, K., N. Tanaka, T. Nakano, E. Kakazu, Y. Kondo, J. Inoue, M. Shiina, K. Fukushima, T. Hoshino, K. Sano, et al. 2010. Exosome secretion of dendritic cells is regulated by Hrs, an ESCRT-0 protein. *Biochem. Biophys. Res. Commun.* 399:384–390. http://dx.doi.org/10.1016/j.bbrc.2010.07.083

Tanaka, T., and A. Nakamura. 2008. The endocytic pathway acts downstream of Oskar in *Drosophila* germ plasm assembly. *Development*. 135:1107–1117. http://dx.doi.org/10.1242/dev.017293

Tavoosidana, G., G. Ronquist, S. Darmanis, J. Yan, L. Carlsson, D. Wu, T. Conze, P. Ek, A. Semjonow, E. Eltze, et al. 2011. Multiple recognition assay reveals prostasomes as promising plasma biomarkers for prostate cancer. *Proc. Natl. Acad. Sci. USA*. 108:8809–8814. http://dx.doi.org/10.1073/pnas.1019330108

Théry, C., M. Ostrowski, and E. Segura. 2009. Membrane vesicles as conveyors of immune responses. *Nat. Rev. Immunol.* 9:581–593. http://dx.doi.org/10.1038/nri2567

Trajkovic, K., C. Hsu, S. Chiantia, L. Rajendran, D. Wenzel, F. Wieland, P. Schwille, B. Brügger, and M. Simons. 2008. Ceramide triggers budding of exosome vesicles into multivesicular endosomes. *Science*. 319:1244–1247. http://dx.doi.org/10.1126/science.1153124

Tsuneizumi, K., T. Nakayama, Y. Kamoshida, T.B. Kornberg, J.L. Christian, and T. Tabata. 1997. Daughters against dpp modulates dpp organizing activity in *Drosophila* wing development. *Nature*. 389:627–631. http://dx.doi.org/10.1038/39362

Vlassov, A.V., S. Magdaleno, R. Setterquist, and R. Conrad. 2012. Exosomes: current knowledge of their composition, biological functions, and diagnostic and therapeutic potentials. *Biochim. Biophys. Acta*. 1820:940–948. http://dx.doi.org/10.1016/j.bbagen.2012.03.017

Walker, M.J., C.M. Rylett, J.N. Keen, N. Audsley, M. Sajid, A.D. Shirras, and R.E. Isaac. 2006. Proteomic identification of *Drosophila melanogaster* male accessory gland proteins, including a pro-cathepsin and a soluble gamma-glutamyl transpeptidase. *Proteome Sci.* 4:9. http://dx.doi.org/10.1186/1477-5956-4-9

Wegner, C.S., L. Malerød, N.M. Pedersen, C. Progida, O. Bakke, H. Stenmark, and A. Brech. 2010. Ultrastructural characterization of giant endosomes induced by GTPase-deficient Rab5. *Histochem. Cell Biol.* 133:41–55. http://dx.doi.org/10.1007/s00418-009-0643-8

Wolfner, M.F. 1997. Tokens of love: functions and regulation of *Drosophila* male accessory gland products. *Insect Biochem. Mol. Biol.* 27:179–192. http://dx.doi.org/10.1016/S0965-1748(96)00084-7

Zhang, J., K.L. Schulze, P.R. Hiesinger, K. Suyama, S. Wang, M. Fish, M. Acar, R.A. Hoskins, H.J. Bellen, and M.P. Scott. 2007. Thirty-one flavors of *Drosophila* rab proteins. *Genetics*. 176:1307–1322. http://dx.doi.org/10.1534/genetics.106.066761

Corrigan et al, http://www.jcb.org/cgi/content/full/jcb.201401072/DC1

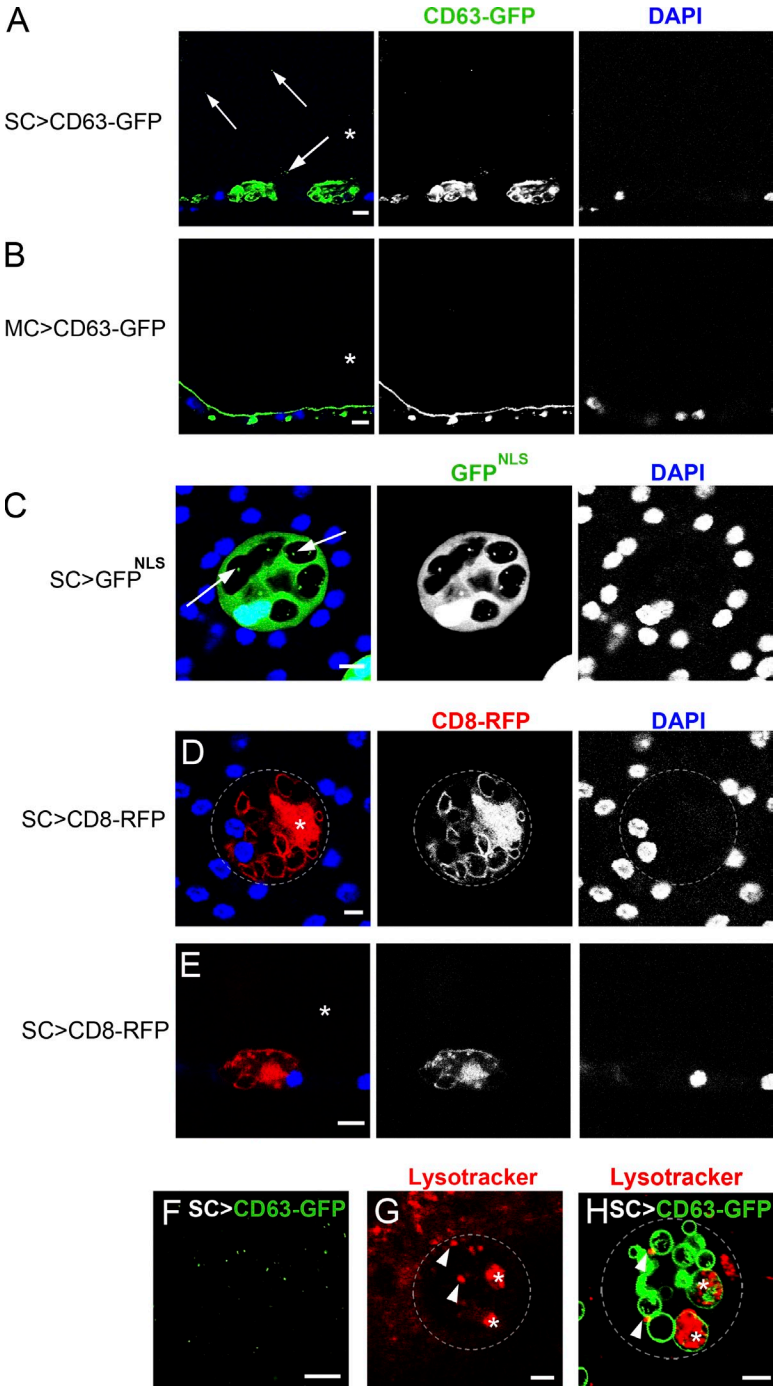

Figure S1. **SCs and not MCs secrete CD63-positive puncta.** (A and B) Transverse sections of AG (in an equivalent focal plane to Fig. 1 C) showing that CD63-GFP is secreted in puncta (arrows; see F for higher magnification image at higher gain setting) into the AG lumen (asterisks) when expressed by SCs (A) but not MCs, imaged here in the middle of the gland where no SCs are present (B). (C) Puncta containing cytoplasmic GFP can also occasionally be seen inside SC vacuoles (arrows) in the surface section. (D and E) CD8-RFP localizes either within (asterisk in D) or at the limiting membrane of large vacuoles (surface section in D) but is not secreted into the AG lumen (asterisk, transverse section in E). (F) Many CD63-GFP–positive puncta secreted by SCs into the AG lumen are detected when the sensitivity and resolution of confocal imaging is increased. (G and H) The w^{1118} (non-GFP marked) control SC (G), imaged live, contains two large (>2 µm, asterisks) and several small (<2 µm, arrowheads) acidic compartments, which stain strongly with LysoTracker red, similar to CD63-GFP–expressing SCs (H). Accurately counting these compartments is not possible because their limiting membranes are not marked. All images show SCs from 3-d-old males incubated at 28.5°C after eclosion. Fixed cell nuclei are stained with DAPI. Approximate outline of cell is marked in D, G, and H. Bars: (A, B, and F) 10 µm; (C–E, G, and H) 5 µm.

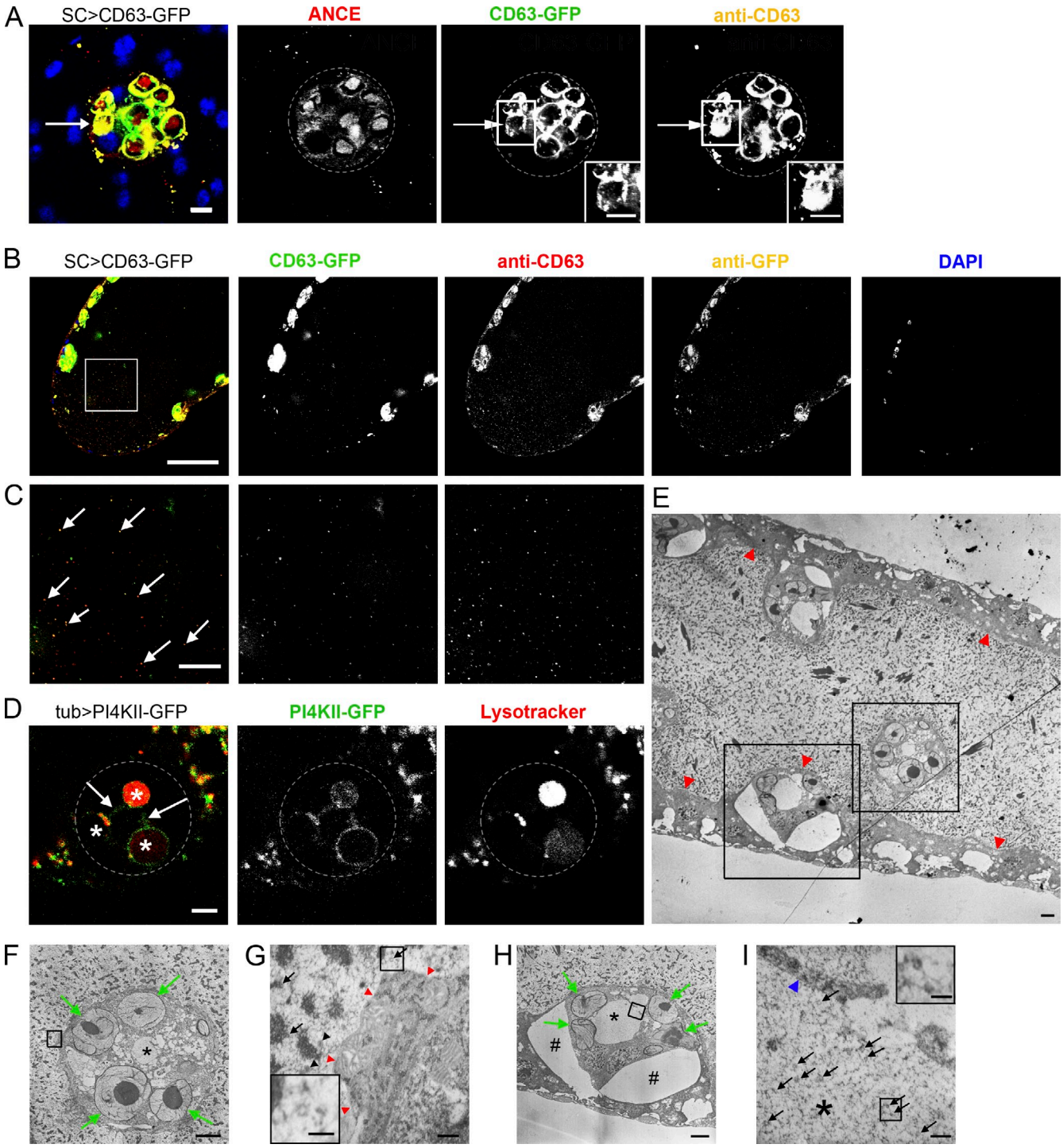

Figure S2. **SCs have large acidic compartments containing internalized CD63-GFP.** (A) A CD63-GFP–expressing SC stained with anti-ANCE and anti-CD63 antibodies reveals one compartment that is filled with CD63 but has low GFP fluorescence (arrows; insets show higher magnification images of boxed regions that include this compartment). This compartment does not contain a dense ANCE core (arrows). (B and C) Transverse section through the lumen of an AG containing CD63-GFP–expressing SCs stained with anti-CD63 and anti-GFP antibodies. Many CD63-GFP fluorescent puncta in the AG lumen colocalize with the anti-CD63 antibody (e.g., arrows in C). C is a higher magnification image of the square outlined in B. (D) Live image of an SC from a *tub-PI4KII-GFP* fly stained with LysoTracker. The late endosome and lysosome marker PI4KII localizes to the limiting membrane of large acidic compartments (asterisks) as well as tubulations extending between them (arrows), which have been observed previously in *Drosophila* salivary gland cells (Burgess et al., 2012). (E–I) Electron micrographs of virgin w^{1118} male AGs. MCs (apical membranes marked with red arrowheads in E) make up the majority of the monolayered epithelium; SCs (boxed in E) are dispersed between MCs, bulge into the lumen, and can be seen in transverse (e.g., cell in H) or surface (e.g., cell protruding into lumen in F) section. SCs contain SVs, comprising an electron-dense core and fibrillar material (F and H, green arrows) and one or two large and less electron-dense, non-SV compartments (F and H, asterisks; H shown at high magnification in I), which by a process of elimination, must represent the large acidic compartments seen in live confocal imaging. The AG lumen contains a range of secreted structures (E), including putative membrane-bound vesicles (G, closed arrows and arrowheads; red arrowheads mark apical surface of epithelium), some of which (G, closed arrows; boxed area enlarged in inset) resemble the ~40-nm vesicles (I, arrows; enlarged in inset) observed inside the large multivesicular compartments in SCs (I, asterisk). These compartments therefore appear to be the counterparts of much smaller mammalian MVBs. F and H are higher magnification images of the boxed regions in E; G and I show higher magnification images of the regions boxed in F and H, respectively. All images show SCs from 3-d-old males incubated at 28.5°C after eclosion. Note that despite attempting several fixation protocols, we were unable to prevent spaces forming at high frequency between SC and MC plasma membranes in the epithelium (# in H). Preservation of compartment membranes was also not optimal (e.g., blue arrowhead in I). Approximate outline of cell is marked in A and D. Bars: (A [main images and insets] and D) 5 µm; (B) 50 µm; (C) 10 µm; (E, F, and H) 2 µm; (G and I, main images) 200 nm; (G and I, insets) 100 nm.

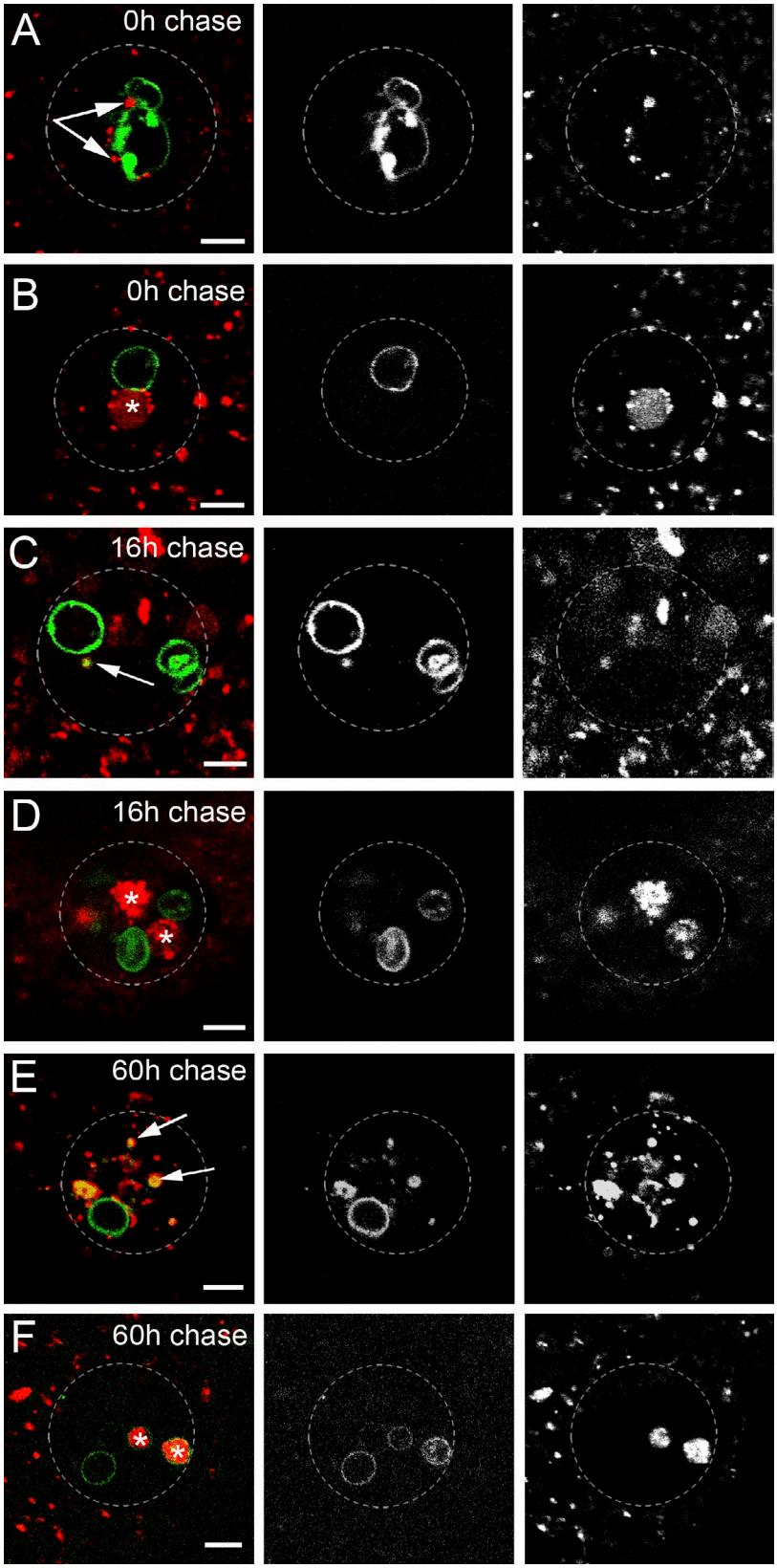

Figure S3. **Analysis of CD63-GFP trafficking and internalization in mMVBLs.** Images from Fig. 3 showing individual color channels: an 8-h pulse of CD63-GFP (induced by inhibition of GAL80^{ts} at 28.5°C) was chased at 18°C for 0–60 h, and proportions of cells with one or more LysoTracker red–positive iLEs (arrows in A, C, and E) and mMVBLs (asterisks in B, D, and F), which were CD63-GFP positive, were determined. The rate of CD63 traffic into endolysosomes is not identical in all cells (Fig. 3 G). Note that when the temperature is shifted down at the end of the pulse, transcripts encoding CD63-GFP are not immediately degraded, so new protein will continue to be made, potentially explaining the persistence of GFP fluorescence in SVs and iLEs. Approximate outline of cell is marked. Bars, 5 µm.

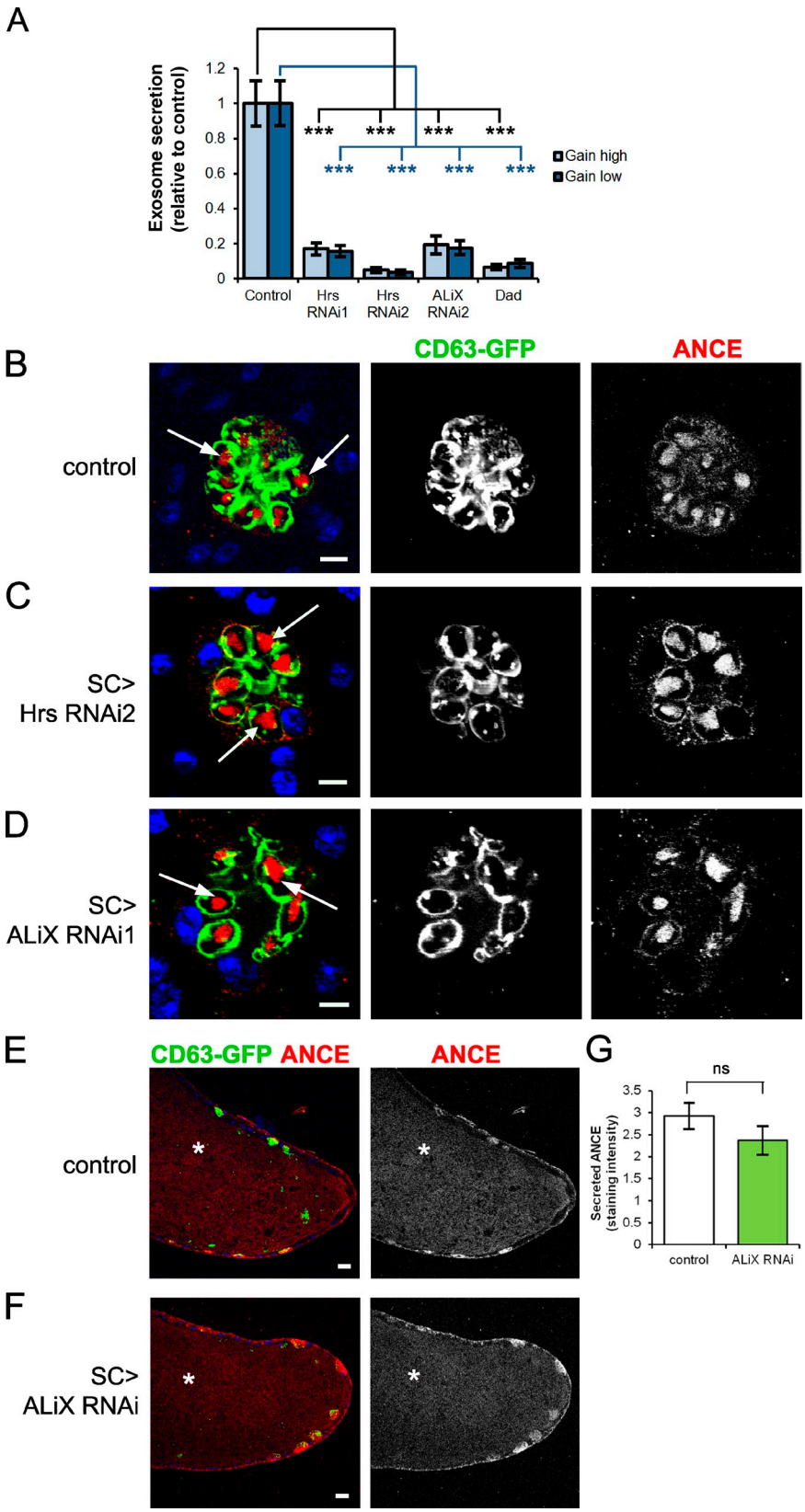

Figure S4. **Blocking ESCRT function in SCs does not affect ANCE secretion.** (A) Relative numbers of SC-expressed CD63-GFP–positive puncta in the AG lumen were quantified for *SC>Hrs-RNAi*, *SC>ALiX-RNAi*, and *SC>Dad* males compared with control males at two confocal gain settings that altered absolute counts by approximately twofold. No effect on relative levels was observed. (B–E) ANCE, which normally localizes to the dense core of control SC SVs (B, arrows) and is secreted into the gland lumen (E, asterisks) but is not detectably expressed in MCs, does not show altered subcellular localization in *Hrs-RNAi*– or *ALiX-RNAi*–expressing SCs (C and D, respectively, arrows). DAPI stains nuclei (blue). (E–G) There is no significant difference in the level of diffuse staining for ANCE in the AG lumen (E and F, asterisks) when *ALiX* is knocked down in SCs (F and G), as measured by calculating the mean signal intensities of three stacked confocal images from the AG lumen taken at 5-µm intervals. Control and *SC>ALiX-RNAi* males were subjected to the same mating protocol as in A, whereas B–D were obtained from virgin males. Data in A and G were analyzed using an unpaired two-tailed Student's *t* test (***, $P < 0.001$, $n > 11$) after the Shapiro–Wilk test to confirm normality. Error bars indicate ±SE. Bars: (B–D) 5 µm; (E and F) 20 µm.

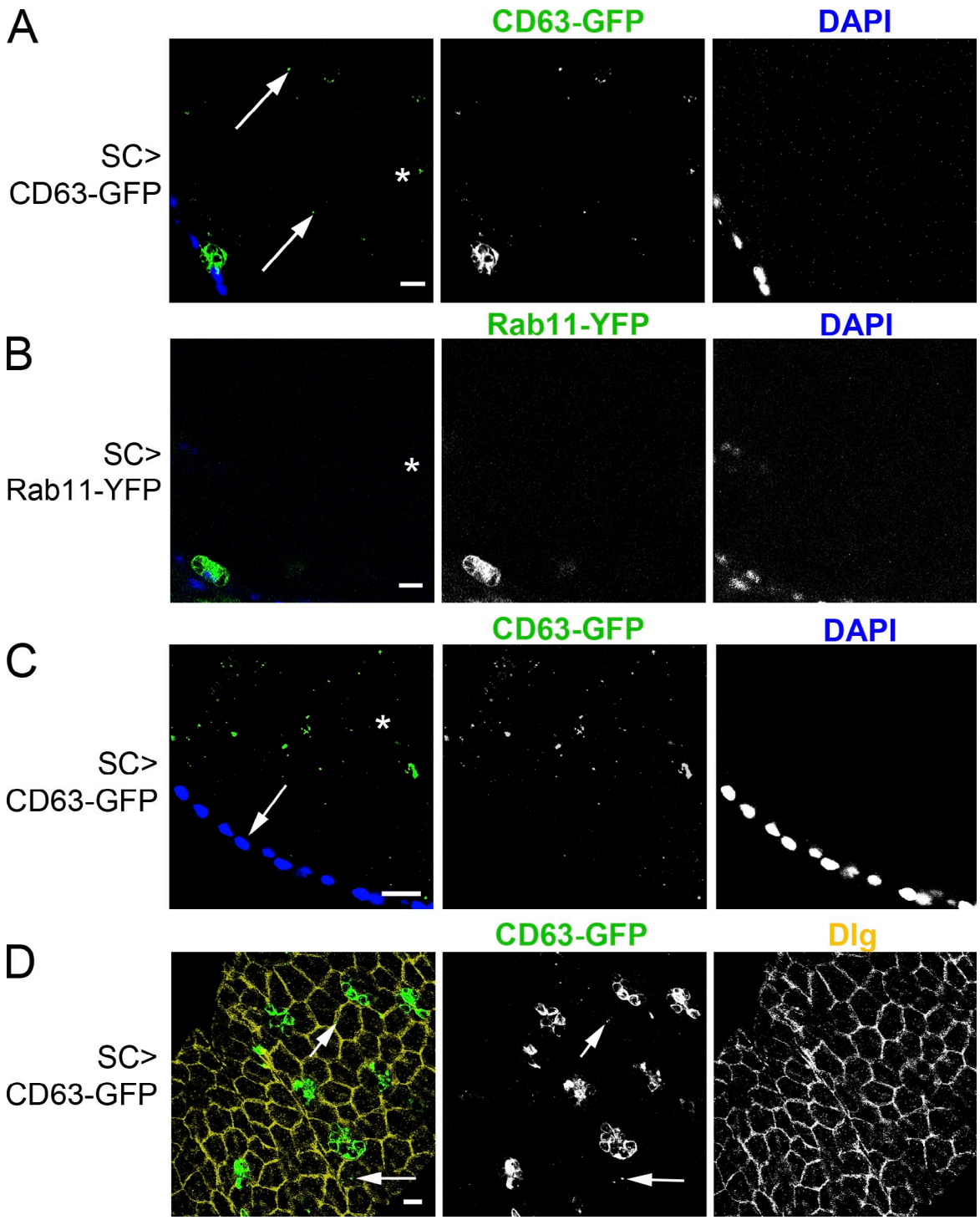

Figure S5. **SC-specific CD63-GFP is transferred to neighboring MCs, but Rab11-YFP is not secreted.** (A and B) Analysis of Rab11-YFP and CD63-GFP secretion when expressed in SCs. Unlike CD63-GFP (A, arrows), YFP-tagged Rab11 is not secreted by SCs, even when highly overexpressed under GAL4 control (B). Images show transverse sections including the lumen (A and B, asterisks) and SCs from 3-d-old males. (C) Transverse section showing no obvious interaction can be seen between CD63-GFP–positive exosomes and the apical surface of MCs (arrow; the asterisk marks the lumen) in most of the AG at 3 d. (D) However, GFP is internalized by the MCs surrounding SCs (arrows). discs large (Dlg) marks apically positioned lateral septate junctions between MCs (junctions between MCs and larger SCs are more apical). DAPI stains nuclei. Bars, 10 µm.

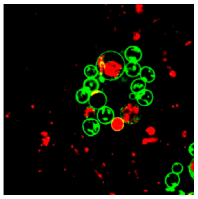

Video 1. **Acidic mMVBLs fuse to nonacidic SVs in SCs.** SC from a 2-d-old male expressing CD63-GFP (green) and stained with LysoTracker red was imaged by time-lapse confocal microscopy using a laser-scanning confocal microscope (LSM 510; Carl Zeiss). Frames were taken every 13.6 s. Stills from this video are shown in Fig. 4 A. Video was produced over a 5-min period. Note how CD63-GFP appears to be transferred to the limiting membrane of the mMVBL at the moment of fusion.

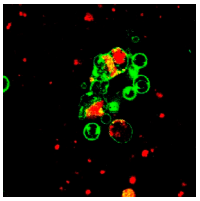

Video 2. **mMVBLs contain CD63-GFP–positive invaginations and acidic microdomains inside mMVBLs.** SC from a 2-d-old male expressing CD63-GFP (green) and stained with LysoTracker red was imaged by time-lapse confocal microscopy using a laser-scanning confocal microscope (LSM 510; Carl Zeiss). Frames were taken every 16.3 s. Stills from this video are shown in Fig. 4 B. Note one CD63-GFP–positive invagination appears to form an ILV-like punctum. A line of peripheral acidic microdomains appears after this event either de novo or through imaging a slightly different plane of the section in the mMVBL. The video was produced over a 5-min period.

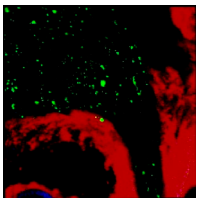

Video 3. **CD63-GFP exosomes may fuse with unmarked sperm tails in females.** Rotating 3D projection of a confocal z stack including the image shown in Fig. 6 D. A z series was collected using a laser-scanning confocal microscope (LSM 510; Carl Zeiss) and the rotating 3D projection movie was recorded using ImageJ 3D Viewer. Note the presence of extended strands of GFP fluorescence and some parallel pairs of short GFP-positive lines that presumably surround sperm tails to which exosomes have recently fused (marked in Fig. 6 D). The female reproductive tract epithelium is marked with CD8-RFP.

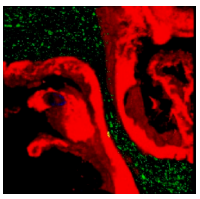

Video 4. **Accumulation of CD63-GFP exosomes along the surface of the female reproductive tract epithelium.** Rotating 3D projection of a confocal z stack including the image shown in Fig. 7 B, highlighting a single GFP-positive interaction site at the epithelial surface that is marked in this figure. A z series was collected using a laser-scanning confocal microscope (LSM 510; Carl Zeiss), and the rotating 3D projection video was recorded using ImageJ 3D Viewer. The female reproductive tract epithelium is marked with CD8-RFP.

Reference

Burgess, J., L.M. Del Bel, C.-I.J. Ma, B. Barylko, G. Polevoy, J. Rollins, J.P. Albanesi, H. Krämer, and J.A. Brill. 2012. Type II phosphatidylinositol 4-kinase regulates trafficking of secretory granule proteins in *Drosophila*. *Development*. 139:3040–3050. http://dx.doi.org/10.1242/dev.077644